Portable Wireless Sensors for

Personal Exposure and Environmental Monitoring

by

Cheng Chen

A Dissertation Presented in Partial Fulfillment
of the Requirements for the Degree
Doctor of Philosophy

Approved July 2014 by the
Graduate Supervisory Committee:

Nongjian Tao, Chair
Sayfe Kiaei
YanChao Zhang
Tsing Tsow

ARIZONA STATE UNIVERSITY

August 2014

ABSTRACT

Monitoring of air pollutants is critical for many applications and studies. In order to access air pollutants with high spatial and temporal resolutions, it is necessary to develop an affordable, small size and weight, low power, high sensitivity and selectivity, and wireless enable device that can provide real time monitoring of air pollutants. Three different kind of such devices are presented, they are targeting environmental pollutants such as volatile organic components (VOCs), nitrogen dioxide (NO2) and ozone. These devices employ innovative detection methods, such as quartz crystal tuning fork coated with molecularly imprinted polymer and chemical reaction induced color change colorimetric sensing. These portable devices are validated using the gold standards in the laboratory, and their functionality and capability are proved during the field tests, make them great tools for various air quality monitoring applications.

ACKNOWLEDGMENTS

I would like to thank my advisor Prof. Nongjian Tao for his guidance and support. Not only he taught me about the research, but also helped me to improve the thinking, communication and leadership skills. I appreciate the opportunity he provided me in attending conferences.

I would like to thank Prof. Erica Forzani for her guidance and help to my research in the laboratory, and during all the field tests.

I would like to thank Prof. Sayfe Kiaei and Prof. YanChao Zhang. I am grateful to have them in my committee.

I would like to thank Prof. Tsing Tsow, Prof. Xiaojun Xian and Prof. Rodrigo Iglesias, their experience and knowledge in the field of electrical and chemistry helped a lot in my research.

I would like to thank all of my past and present peers in Prof. Tao’s group. Friendship and support from all the peers is greatly appreciated.

Most importantly, I would like to thank my family for their tremendous support over the years.

Funding was provided by NIEHS/NIH via the Genes, Environment and Health Initiative (GEI) program.

TABLE OF CONTENTS

CHAPTER Page

LIST OF TABLES

LIST OF FIGURES

Figure Page

Figure Page

CHAPTER 1

INTRODUCTION

1.1 Background

Volatile organic compounds (VOCs), including aromatic and chlorinated hydrocarbons, have serious environmental and health impacts [1]-[2]. Human exposure to VOCs has become an important public health concern. VOCs exists both indoor and outdoor, with indoor concentration usually higher than the outdoor concentration. The main source of outdoor VOCs is the on road vehicle emissions and the industrial solvent usage [3]-[5], and the indoor VOCs source including paints, furniture, nail polish, printers and so on. A group of VOCs including benzene, toluene, ethyl benzene and xylenes, collectively known as BTEX, are of great concern of many epidemiologists. These VOCs are defined as class A pollutants by US Environmental Protection Agency (EPA) because they are potential carcinogens, and many cause leukemia, lymphomas and other diseases [6]-[13].

Even though the health impact of the VOCs is recognized, the most commonly used method for monitoring VOCs involve a sample collection followed by a gas chromatography and mass spectrometry test. It is expensive and time consuming. In order to assess VOCs concentration with high spatial and temporal resolutions at personal level, an affordable, low power, small size, light weighted, high sensitivity and selectivity device with wireless communication capability is much needed.

Electrochemical sensors are usually commercialized as convenient portable gas monitors, their target analytes include oxygen, carbon monoxide, hydrogen sulfide and sulfur dioxide [14]-[15]. However, these sensors are not able to detect the BTEX.

Different detection methods combine with gas chromatograph (GC) is another approach. These detection methods include thermal conductivity (TCD) [16], photoionization (PID) [17]-[18], flame ionization (FID) [17], electrochemical [14], [19], and surface acoustic wave (SAW) sensors [20]. Micro machined columns and preconcentrators have been integrated with SAW and chemresistor detectors [21]. Portable GCs offer great capability and flexibility for epidemiological, environmental and safety applications. However, the micro fabricated GCs are still under development phase and the cost of tiny components seems to be higher than conventional parts. Commercially available GCs are still expensive, range from several to tens of thousands dollars), and not suitable for epidemiological studies.

1.2 Tuning fork sensor platform

Microfabricated quartz crystal tuning fork have been using in many applications which require precise timing, including wristwatch and microcontroller integrated circuit. Quartz is a piezoelectric material which means application of mechanical stress results in generation of an electrical signal and vice-versa, and that's the basic principle used in the operation of the quartz tuning fork. The commercial quartz tuning fork are built in a way that the fragile prongs are protected in a metal can; this can also protect the prongs from outside pressure variation and other potential disturbances. Mechanical resonations are generated when a voltage is applied the prongs. The tuning forks require very low power consumption and are very stable and precise.

An important feature of the tuning fork is the high quality factor Q (ratio of energy stored to energy dissipated per oscillation), and this make it suitable for frequency-based measurements. Resonant frequency of a tuning fork can be expressed as follows:

$$f_0 = \frac{1}{2\pi}\sqrt{\frac{k'}{M}}$$

Where *k* represents effective spring constant and *m* is mass of the tuning fork. The typical Q factor of a tuning fork is 10,000 in the air. In order to use tuning fork as chemical sensor, it need to be modified. We removed the metal can enclosing the prongs, exposing the prongs of the tuning fork. Then, the tuning fork prongs are modified to be hydrophobic, and coated with molecular imprinted polymer. The molecular imprinted polymer forms a thin layer on the prongs, and binds with the target analyte. Once the analyte is bound with the polymer on the prongs, the mass of the prongs increase and therefore decrease the resonant frequency. The change of the frequency is given by:

$$\Delta f(k', M) = (\frac{f_0}{2})[\frac{\delta k'}{k'} - \frac{\delta M}{M}]$$

And based on the mass change, the concentration of the target analyte can be calculated. These commerically avaible (US $0.01/each) tuning forks is a great for portable chemical sensors.

1.3 References

[1] Amorim, Leiliane CA, Joana P. Carneiro, and Zenilda L. Cardeal. "An optimized method for determination of benzene in exhaled air by gas chromatography–mass spectrometry using solid phase microextraction as a sampling technique." *Journal of Chromatography B* 865.1 (2008): 141-146.

[2] Sexton, Ken, et al. "Children's exposure to volatile organic compounds as determined by longitudinal measurements in blood." *Environmental health perspectives* 113.3 (2005): 342.

[3] Han, Xianglu, and Luke P. Naeher. "A review of traffic-related air pollution exposure assessment studies in the developing world." *Environment international* 32.1 (2006): 106-120.

[4] Buczynska, Anna Jolanta, et al. "Atmospheric BTEX-concentrations in an area with intensive street traffic." *Atmospheric Environment* 43.2 (2009): 311-318.

[5] Ablat, Hayrensa, et al. "Nafion film/K+-exchanged glass optical waveguide sensor for BTX detection." *Analytical chemistry* 80.20 (2008): 7678-7683.

[6] De Medeiros, A. P., et al. "Traffic-related air pollution and perinatal mortality: a case-control study." *Environ Health Perspect* 117.1 (2009): 127-132.

[7] Fondelli, M. Cristina, et al. "Benzene exposure in a sample of population residing in a district of Florence, Italy." *Science of the total environment* 392.1 (2008): 41-49.

[8] Harrison, Roy M., et al. "Analysis of incidence of childhood cancer in the West Midlands of the United Kingdom in relation to proximity to main roads and petrol stations." *Occupational and Environmental Medicine* 56.11 (1999): 774-780.

[9] Raaschou‐Nielsen, Ole, and Peggy Reynolds. "Air pollution and childhood cancer: a review of the epidemiological literature." *International journal of cancer*118.12 (2006): 2920-2929.

[10] Tsai, S., H. Weng, and C. Yang. "Association of Childhood Leukemia with Residential Exposure to Petrochemical Air Pollution in Taiwan." *Epidemiology*19.6 (2008): S292.

[11] Weng, Hsu-Huei, et al. "Childhood leukemia and traffic air pollution in Taiwan: petrol station density as an indicator." *Journal of Toxicology and Environmental Health, Part A* 72.2 (2008): 83-87.

[12] Whitworth, Kristina W., Elaine Symanski, and Ann L. Coker. "Childhood lymphohematopoietic cancer incidence and hazardous air pollutants in southeast Texas, 1995–2004." (2008).

[13] Infante-Rivard, Claire. "Chemical risk factors and childhood leukaemia: a review of recent studies†." *Radiation protection dosimetry* 132.2 (2008): 220-227.

[14] http://www.raesystems.

[15] www.draeger.com

[16] www.agilent.com/chem/microgc.

[17] www.hnu.com.

[18] www.photovac.com.

[19] http://microsensorsystems.com.

[20] http://www.estcal.com.

[21] Lu, Chia-Jung, et al. "First-generation hybrid MEMS gas chromatograph." *Lab on a Chip* 5.10 (2005): 1123-1131.

CHAPTER 2

A WIRELESS HYBRID CHEMICAL SENSOR FOR DETECTION OF ENVIRONMENTAL VOLATILE ORGANIC COMPOUNDS

Abstract

A wireless hybrid device for detecting volatile organic compounds (VOCs) has been developed. The device combines a highly selective and sensitive tuning-fork based detector with a pre-concentrator and a separation column. The selectivity and sensitivity of the tuning-fork based detector is optimized for discrimination and quantification of benzene, toluene, ethyl benzene, and xylenes (BTEX) via a homemade molecular imprinted polymer, and a specific detection and control circuit. The device is a wireless, portable, battery-powered, and cell-phone operated device. The device has been calibrated and validated in the laboratory and using selected ion flow tube mass spectrometry (SFIT-MS). The capability and robustness are also demonstrated in some field tests. It provides rapid and reliable detection of BTEX in real samples, including challenging high concentrations of interferents, and it is suitable for occupational, environmental health and epidemiological applications.

2.1 Introduction and background

2.1.1 Introduction

Human exposure to toxic chemical has become an important problem of public health. Many of these toxic chemicals are volatile organic compounds (VOCs). A group of VOCs include benzene, toluene, ethyl benzene and xylenes, collectively known as BTEX, which are of great concern of many epidemiologists. The main source of BTEX emission (more than 80 %) are automobile exhaust and other traffic related sources [3, 9, 11], indoor sources consist of commonly used paint, detergent, nail polish. Typical BTEX concentrations range from low parts per billion (ppb) by volume [3, 10] to low parts per million (ppm) by volume levels [11]. These VOCs are defined as class A pollutants by US Environmental Protection Agency (EPA) because they are potential carcinogens (US EPA), and many cause leukemia, lymphomas and other diseases [1, 2, 4-9]. Therefore, detection and quantification of trace level BTEX in the air can be critical for many applications, including occupational health, industrial safety, epidemiological study and environmental monitoring. Up to date, gas chromatography and mass spectrometry (GC/MS) is the main technology of VOCs measurement in the air. The sample collection site and the analysis laboratory are usually at different locations, thus sampling collection

using canister, Tedlar bag and adsorbent tube are involved in almost all the GC/MS related VOCs measurement, and are at risk for sample contamination and loss during storage and transportation. The high cost and long turnaround time limit the data collection in field investigations.

2.1.2 Gas chromatography and mass spectrometry

As we mentioned above, GC/MS is up to date the most common way of analyzing VOCs in a complex mixture. Gas chromatography is a common separation technology used in analytic chemistry. In gas chromatography, a mixture sample with different compounds is injected to a column, the mobile phase is the carries gas, and the stationary phase is a thin layer coating inside the capillary column. As the mobile phase moves along the stationary phase, different compound will be having different interaction with the stationary phase. Depend on how strong the interaction is, the compounds will move in the column at a different speed, result in a different retention time (the time a compound take between the injection and elution), which can be used to characterize the compound. Gas chromatography is usually coupled with mass spectrometry (MS). When a sample is loaded into the MS instrument, the compounds are ionized and then separated according to their mass-to-charge ratio in electromagnetic field. The ions then are detected and a mass spectrum is made from the signals.

2.1.3 Portable chemical sensor for VOCs analysis

While reliable, Conventional GC/MS measurement is expensive, not real-time, and often required a trained technician. The tasks of analyzing VOCs in a complex

mixture of many interferents with a high sensitivity and selectivity inexpensive portable chemical sensor in real time, is still a challenge. There are two common approaches for developing a chemical sensor which can detect target analyte in a complex mixture. One common approach of target detection with the present of interferents makes the use of the specific binding between a probe and a target molecule. A strong binding of a probe and a molecule usually results in a high sensitivity, but also means a slow response time and low recovery rate, which requires long sampling time and frequently replacing the sensor, thus not a good candidate for real time detection. Another strategy is gas chromatography technology; a widely used technique is gas chromatography/mass spectrometry (GC/MS). Measurement of VOCs with GC/MS involves the sample collection using canister, Tedlar bag and adsorbent tube, the detection is not real-time and the cost is substantial. And obviously a bulky and expensive instrument is not suitable for real-time field testing. Commercial portable GC systems have been developed and marketed [12]-[16], but their sensitivity is limited. Carrier gas and computers are needed in some systems and the cost is still high. A miniaturize GC system consists of capillary column, a microfabracated preconcentrator and chemresistor or surface acoustic wave (SAW) detectors has been reported [17], [18]; The combination of microfabracated GC column and metal oxide(MOX) gas sensors has also been developed [19], [20].

2.1.4 Quartz crystal tuning fork as chemical sensor

Microfabricated quartz crystal tuning fork have been using in many applications which require precise timing, including wristwatch and microcontroller integrated circuit. Quartz is a piezoelectric material which means application of mechanical stress results in

generation of an electrical signal and vice-versa, and that's the basic principle used in the operation of the quartz tuning fork. The commercial quartz tuning fork are built in a way that the fragile prongs are protected in a metal can; this can also protect the prongs from outside pressure variation and other potential disturbances. Mechanical resonations are generated when a voltage is applied the prongs. The tuning forks require very low power consumption and are very stable and precise.

An important feature of the tuning fork is the high quality factor Q (ratio of energy stored to energy dissipated per oscillation), and this make it suitable for frequency-based measurements. Resonant frequency of a tuning fork can be expressed as follows:

$$f_0 = \frac{1}{2\pi}\sqrt{\frac{k'}{M}}$$

Where *k* represents effective spring constant and *m* is mass of the tuning fork. The typical Q factor of a tuning fork is 10,000 in the air. In order to use tuning fork as chemical sensor, it need to be modified. We removed the metal can enclosing the prongs, exposing the prongs of the tuning fork. Then, the tuning fork prongs are modified to be hydrophobic, and coated with molecular imprinted polymer. The molecular imprinted polymer forms a thin layer on the prongs, and binds with the target analyte. Once the analyte is bound with the polymer on the prongs, the mass of the prongs increase and therefore decrease the resonant frequency. The change of the frequency is given by:

$$\Delta f(k', M) = (\frac{f_0}{2})[\frac{\delta k'}{k'} - \frac{\delta M}{M}]$$

To overcome the difficulties of the current detection technologies, we have recently demonstrated a hybrid approach that integrates specific binding (e.g.,

colorimetry) and selective separation (e.g. GC) of analytes [21]. The work confirmed the value of the hybrid approach, however, the sensitivity and selectivity fall short to meet the needs of environmental monitoring. In the present work, we introduced adsorbent packed preconcentrator that selectively collects and release analytes, a more sensitive microfabricated tuning fork sensor, an automated heat and flow control with a microcontroller-based circuit, and wireless communication with a cell phone. We have also integrated all the components into a single unit that weighs about 1.2 lbs., tested its analytical performance, and validated its usability in various real world scenarios. The device can reliably detect a few ppb-level of BTEX in complex real samples within minutes, more than three orders of magnitude improvement over the previous work. The system schematic and the performance of the key components of this device are described below.

2.2 Prototype Description and Experimental Methods

In this hybrid chemical sensor device, three key components are combined: 1) specific pre-concentration for sample collection, 2) chromatographic separation for discrimination of interferents and target analytes, and 3) specific binding for detection of analytes. A distinctive feature of the device is a highly selective tuning-fork based detector. The portable hybrid device can detect VOCs in real-time at few part per billion-levels. While the new detector allows sensitivity, specificity and low size, the preconcentration and separation further improves the selectivity in complex analysis environments. In addition, the device is rechargeable battery-operated and paired to a Smartphone App via a wireless connection, which further reduces weight burden and size.

A built-in Bluetooth chip in the hybrid device enables connectivity with a Bluetooth in the cell phone, which not only allows data retrieval from the device to the cell phone, but also remote control of the device from the cell phone. To introduce the working principle of the chemical sensor, we first present the key components, and then briefly describe the measurement procedure.

A. The Quartz Crystal Tuning Fork Sensor

Quartz crystal tuning forks are mechanical resonators which have a resonance frequency of 32.768 KHz (Newark Electronics) with high quality factor (about 10000 in ambient air) and high sensitivity of mass detection (4pg/mm2) [22]-[25]. They also have low power consumption (1 μW maximum) and a small size (0.1×0.5×3 mm3). A digital counter build in the circuit is used to measure the tuning fork frequency change at a 1.8 mHz resolution. To achieve the desired sensitivity and selectivity, the tuning forks are modified with molecular imprinted polymer (MIP). MIP is highly cross-linked polystyrene formed by divinylbenzene, synthesized with biphenyl as template and xylenes as porogens. The MIP binding sites bind with the hydrocarbons mainly through π- π interactions and van der Waals interactions, results in a selective and reversible sensing. The tuning fork prongs need to be hydrophobic so that the MIP can effectively stick to the prongs. To make the tuning fork hydrophobic, the prongs are first soaked in the Phenyl trimethoxy Silane, and then in dodecane ethiol. A MIP-coated tuning fork with ppb-level detection limits for common hydrocarbons like xylenes and toluene is typical. Figure. 2-2(a) shows a tuning fork sensitivity test. In this test, 250 ppb xylene is prepared and injected to the tuning fork sensor cartridge. The sensor signal is 0.168 Hz,

while the noise level is as low as 0.001 Hz. The detection limit is then determined by signal at 3 times of the noise level, which is about 4.4 ppb for xylenes. The sensor also shows a rapid response time and fast desorption process, which are very critical for real-time detection. Figure. 2-2(b) shows a reproducibility test, in which the tuning fork sensor is exposed to the same concentration analyte for 12 complete measurement cycles. The mean of the responses is 0.26048 Hz, while the standard deviation is 0.00778 Hz, which is about 3% error. Overall, the sensor shows a fast response time, rapid desorption process and excellent reproducibility, together with the low power consumption and super small size features, the tuning fork sensor is a suitable for portable chemical sensor and real-time detection. Common interferents including acetone, ethanol and ammonia that have been tested at high concentrations (42ppm) shows no response on the MIP-coated tuning fork sensor [26]. The tuning fork sensor used in this hybrid chemical sensor device is after the gas chromatography capillary column, plugged into the circuit board. It is protected inside a Teflon chamber with a very small dead volume which is only 12 μL. The plug and play feature of the tuning fork sensor makes it easy to change and maintain.

B. The Preconcentrator

The preconcentrator located before the gas chromatography column, incoming samples will first go through the preconcentrator and get trapped. It is constructed from a stainless steel tube with a size of 1/16 inch diameter and 2.5 cm length. Packed adsorbent is retained with two glass fiber plug. A Nichrome heating wire which has a resistance of 4 ohms is coiled around the stainless steel tube. The adsorbent can absorb the VOCs at room temperature; a voltage is applied to the heating wire to heat the preconcentrator to a desired high temperature (300 °C) during desorption stage and injection stage. The

adsorbent material is the key component in the preconcentrator, and a very important property of the adsorbent material is the capacity. We reviewed adsorbent properties and three different materials are tested. These three materials are Carbopack X, Carbopack B and Carboxen 1016 with surface area of 100 m^2/g, 240 m^2/g and 75 m^2/g respectively. Carbopack B and Carbopack X are graphitized carbon blacks; Carbopack B is non-porous while Carbopack X is porous. Carboxen 1016 is carbon molecular sieve which is the carbon skeletal framework remaining after the pyrolysis of a polymer precursor. A gas sample of toluene at the concentration of 10 ppm is used to compare the breakthrough volume between these three compounds. A miniature pump brings the gas sample which is a 10 ppm toluene into the preconcentrator; a MIP-coated tuning fork sensor with circuits is located at the outlet of the preconcentrator. At room temperature, the adsorbents inside the preconcentrator can absorb the toluene, therefore, as long as the adsorbent materials are not saturated, the toluene can't go through the preconcentrator or reach the tuning fork sensor. Therefore the sensor should not show any positive response of toluene until saturation of the preconcentrator is reached. In the experiments, each material is tested with the same amount which is 12 mg. The flow rate of the toluene gas sample is also the same, which is 700 mL/min. By comparing the time from the point of sample injection to when the sensor starts to show response, we can compare the capacity of each adsorbent material. The responses of the tuning fork for each adsorbent are shown in Figure. 2-3. It can be observed from Figure. 2-3 that the breakthrough time are 11.5 minutes, 2.5 minutes and 3 minutes for Carbopack X, Carbopack B and Carboxen 1016, respectively. Carbopack X has longest saturation time, and therefore it has the largest capacity. This is mainly due to the porous property and its high surface area.

An important parameter that describes how efficient the pre-concentrator traps and desorbs the analytes is pre-concentration factor. In our hybrid device, the factor is defined as the ratio of the tuning fork sensor response of a sample injection using the preconcentrator to that of a direct sample injection without using the preconcentrator. Figure. 2-4(a) shows the tuning fork sensor response of a direct injection of 10 ppm BTEX sample, and Figure. 2-4(b) shows the response of a 20 ppb BTEX injection after 20 minutes of pre-concentration. The corresponding pre-concentration factor is ~800 for BTEX. This large preconcentration factor not only reflects the high trap efficiency, but also is a result of high desorption efficiency. We have tested and found that desorption efficient is as high as 99.2%, which is important for repeated detection and analysis of samples. Chemical sensors based n specific molecular binding in general lack this capability for repeated measurements.

C. The Gas Chromatography Capillary Column

The MIP-coated tuning fork sensor provides a selective detection over hydrocarbons family, but including an additional separation mechanism to further improve the selectivity of the system is still desirable. The gas chromatography capillary column located after the preconcentrator and before the tuning fork detector. Two kinds of gas chromatography columns whose stationary phase material are carbowax and cyanopropylphenylsilicone are coupled together to provide the optimal separation. The column with a carbowax stationary phase is UAC-CW (Quadrex) and the column of cyanopropylphenylsilicone is UAC-502 (Quadrex). 2 meters of each column are coupled together, and implemented into the system. The use of the relativity short column

provides a fast gas chromatography measurement while still ensure sufficient separation over BTEX compounds. A typical chromatogram of the BTEX separation corresponding to an injection of subnanomole amount of BTEX mixture for 5 seconds is shown is Figure. 2-4(b), a complete separation analysis of BTEX only takes 200 seconds, a MIP-coated tuning fork sensor is served as the detector in this test. While providing a fast separation of BTEX, the 4 meters columns sometimes don't have enough capability to separate a very complicated sample. Longer column usually provide a better separation, but the analysis time will also increase significantly. There is a trade-off between the separation efficiency and analysis time, and with the easiness of changing the GC column, different columns can be plugged into this hybrid chemical sensor device to adjust the need of different applications.

D. The circuit

The microcontroller-based circuit in this chemical sensor device is responsible for controlling, measuring and communication. It times and controls the valve switching between the five different operation stages: preconcentration stage, desorption, injection stage, analysis stage and cleaning stage. It also controls turning on or off the heater. The tuning fork is driven by the circuit, and the frequency is measured. The Bluetooth chip is connected to the microcontrollers so that the command can be sent to the circuit, and the data can be send out to the Smartphone user interface.

2.3 Results and Discussion

2.3.1 Prototype Development and Validation

A. Development of the prototype of the hybrid device

The integration of basic components of the hybrid device requires of smart engineering solutions to achieve maximum analytical performance. The analytical performance is evaluated by the capability of the system to separate sample components, and by signal-to-noise ratio quality of each separated component.

Fluids components such as flow rate, dead volumes, materials, and fluid control were optimized and are as follows. First, an optimal flow rate of ~8 mL/s is used to reach good sample component separation, avoiding significant diffusional dispersion of sample components inside the column. Flow conditions are reached via a miniature 5.7-V pump (Parker). Second, dead volumes are minimized via home-made connectors to further decrease sample components dispersion, and separation peak broadening. Third, inert materials (Teflon and stainless steel) are used to prevent uncontrolled adsorption of sample components, excepting the preconcentrator, separation column, and detector. In addition, a zeroing filter based on activated carbon (Purafil) is integrated to generate clean air from ambient air as carrier gas, eliminating the burden of using external carrier gas cylinders, and further minimizing weight and size. Lastly, the hybrid device has a fluid system controlled by four miniature valves (Lee Co.) with work in synergic coordination via a built-in control circuit, which is wirelessly activated and set up from the user interface in the cell phone (Figure 2-1(b) insert). All above-mentioned components are packed together with the pre-concentrator, separation column, detector, and power components (two lithium-ion polymer batteries) into a size of 12.9×9.9×4.9 cm3 project plastic box. The device weights a total of 1.2 lbs. Figure 2-1(a) shows a prototype hybrid device along with the Smartphone user interface. The integration of all

components leads to a truly portable and self-contained hybrid device for trace level VOCs detection in complex mixtures.

B. The user interface and control of hybrid device function

The user interface is developed in a Motorola Q phone via Visual Studio (Microsoft) software. The user interface is another key component of the device. It allows receiving, displaying, and storing device data. Once the data have been acquired, it also allows further data transmission via seamless wireless network. As mentioned before it allows controlling the hybrid device functions and its time settings. The device functions consist of five major stages: 1) pre-concentration, 2) desorption, 3) injection, 4) analysis, and 5) cleaning.

1) Pre-concentration stage: In this stage, the pump provides a constant flow of sample (e.g. indoor or outdoor air) to the pre-concentrator, and VOCs are adsorbed. Preconcentration times are adjusted based on VOC concentrations. Preconcentration times are inversely proportional to concentrations. Typically 9-min preconcentration allow detection of few ppb. Once the pre-concentration time is finished, the valves are switched so that scrubbed clean air is purged into the GC column and tuning fork detector registers a baseline.

2) Desorption stage: After the pre-concentration stage, desorption stage starts with the pre-concentration heating to 300°C for 1 min, which allows VOC desorption and release to the gas phase.

3) Injection stage: After desorption stage, the valves are switched again to a injection stage, and scrubbed (clean) air passes through the heated preconcentrator and takes the VOC vapors to the separation column. The injection stage lasts 15 seconds.

4) Analysis stage: After the 15-sec. injection, the analysis stage follows with the separation of sample components in the column via a clean air carrier active flow. Concurrently, the tuning fork detector measures the sensor signals and sends them to the Smartphone. As the sample components exit the separation column, detection id perform from the recorded peaks in a chromatogram (Figure 2-4(b)).

5) Cleaning stage: After the analysis time is finished, the device will clean up the pre-concentrator with an additional heating step, and flow of clean air so that the device can be ready for the next testing event.

It is important to mention that the above-described operation is fully automatic, and can be initialed by simply push a button in the Smartphone user interface.

C. Laboratory Characterization and Calibration

We have calibrated the hybrid device using BTEX samples with various concentrations. The BTEX samples are prepared and the concentration of each compound is tested with a Selected Ion Flow Tube– Mass Spectrometer (Instrument Science, UK). Figure. 2-5(a) shows a chromatogram for one of BTEX calibration sample. 19 m column is being used in this calibration test. The BTEX components elute at the expected elution

sequence: benzene, toluene, ethylbenzene and xylenes, consecutively. Also note that the xylene isomers which are m-xylene, p-xylene and o-xylene are also well separated. The high separation efficiency allows the device to analyze a complex sample. The calibration curves (Figure. 2-5(b-d)) show that the peak heights of each component are proportional to the analyte concentrations. Notice that the linearity concentration goes up to 900 ppb for benzene, 2400 ppb for toluene and 800 ppb for xylene. The sensitivity factors are found to be 0.57 mHz/ppb, 0.50 mHz/ppb and 1.15 mHz/ppb for benzene, toluene and xylene, respectively. The detection limits are a few ppb for all the compounds. It is important to mention that a short pre-concentration time which is 45 seconds is used here; and the detection limits can be further lowered to about 1 ppb by increasing the pre-concentration time to 5 minutes. These large linear calibration range and low detection limit levels are useful for most of outdoor and indoor environmental air monitoring scenarios, as well as industrial applications, and represent an extraordinary good performance for a portable hybrid sensor device. Once the calibration is established, unknown BTEX concentrations can be determined, using either the peak height or peak area of the chromatograms.

2.3.2 Field testing

In order to test the robustness of the hybrid device in the field, preliminary field tests under different scenarios were carried out and the findings are summarized below.

A. Air quality test during the Gulf oil spill

The Gulf oil spill in 2011 was a disaster to both the human and the environment. While the seawater was contaminated with over 160 billion of oil gallons, an unknown amount of petroleum VOC contaminated the air of the oil spill area and their surroundings, and represented a high concern hazard for the area inhabitants and workers engaged in oil remediation and cleaning activities [27]. Conventional monitoring equipment showed limited sensitivity and slow response time over this emergency [28]. Taking advantage of the portability of the hybrid device, our team rented a shrimp boat and tested air quality in multiple locations in an area located 69 miles from the spill site (Figure. 2-7(b)). For this field test, we used a single 2-m column (UAC-502) and 5 minutes preconcentration time.

A typical data set is shown in Figure. 2-6(a) as a blue curve. For comparison, a 50-ppb BTEX calibration curve (Figure. 2-6(a) black curve) is also plotted in the same figure. The results reveal two important findings. First, peaks associated with BTEX are absent, which indicate their levels are below 1 ppb. This finding is in agreement with the data reported by EPA's mobile units, which were deployed in the area at the time of the analysis (June 13th, 2010). The absence of BTEX in that area is presumably due to the high volatility of the BTEX compounds. Second, a large peak between where toluene and ethyl benzene peaks is found. This peak is due to an alkyl hydrocarbon, and its concentration is estimated to be ~50 ppb. We have confirmed the finding by analyzing water samples collected at the site with GC-MS. The GC-MS data is shown as inset in Figure. 2-6(a), which reveals a peak between toluene and ethyl benzene. This peak is identified as a hexane derivative, which is in excellent agreement with the finding of our hybrid device.

B. BTEX detection in gasoline vapors

Gasoline is a petroleum-derived liquid, which is primarily used as engines fuel. It consists mostly of aliphatic and aromatic hydrocarbons. Gasoline vapor is one of the most complicated real samples [29], and is used to challenge the performance of the hybrid device. Because of the complexity of gasoline vapor, a longer separation column is used to provide better separation. Because of the trade-off between the separation and the analysis time, the latter is increased to 50 minutes. Figure. 2-7(a) shows the chromatogram of a real gasoline vapor. The preconcentration time for this sample is 5 minutes, and the analysis time is 40 minutes. About 20 peaks are observed from the chromatogram, which include the BTEX peaks. Benzene is shown in Figure. 2-7(b). Figure. 2-7(c) and Figure. 2-7(d) present the peaks of toluene and xylenes respectively. Ethyl benzene, m-xylene, p-xylene and o-xylene are also separated in this case. The concentrations of BTEX in this sample are tested using a Selected Ion Flow Tube Mass Spectrometry (Trans Spectra Limited). The ability of the device to detect BTEX in a complex mixture with different kinds of interferents is demonstrated in this test.

2.4 Conclusion

A hybrid chemical sensor device has been developed and validated. The key components of this portable device are a mini adsorbent packed preconcentrator, two series-coupled 2 meters or single 19 meters gas chromatography capillary column, and a novel tuning fork detector coated with molecular imprinted polymer. Filtered ambient air is used as the carrier gas. Other features include Lithium-ion polymer battery power source, a Bluetooth communication chip for remote control of the device and the data

transmission, and an application in Smartphone for remote command sending, data storage, data analysis and figure plotting.

In most of the interesting applications, including indoor and outdoor air quality monitoring, limits of detection for VOCs in the parts per billion range are needed. The use of the adsorbent packed preconcentrator highly improves the sensitivity of the device. The GC column provide the device a chromatography separation, while maintain a fast measurement process. The use of the tuning fork detector is the most unique part of this device, this tuning fork sensor not only provide a sensitive but also a selective detection of VOCs. The device has been calibrated and validated in the lab with different column length configurations. The device is portable, battery operated, and wirelessly connected to a user-friendly cell phone application. Device applications in real world, such as outdoor air quality and BTEX in gasoline vapor detection are demonstrated.

Even though the device has demonstrated its capability, there are improvements need to be done. One concern of the device is the relative long analysis time when equipped a long column. There are several approaches which could address this problem, one possible way is to use a more powerful pump which can provide a higher flow rate; another way is to heat the column. Both will result in an increase of power consumption. Finding a better stationary material to increase the separation efficiency, or using multiple columns in parallel to reduce the pump load and increase the separation efficiency could be solutions, too. MEMS technology could be used to approach these proposals. A microfabricated preconcentrator could be used to reduce the thermal mass and therefore reduce the heater power consumption. Instead of using a plastic box, we could design and machine a box which will be more specific to fit the device components,

therefore decrease the device size and increase the robustness. To summary, future work will aim on making the device more selective, sensitive, and faster and smaller, to provide a really valuable tool for various air quality monitoring applications.

(a)

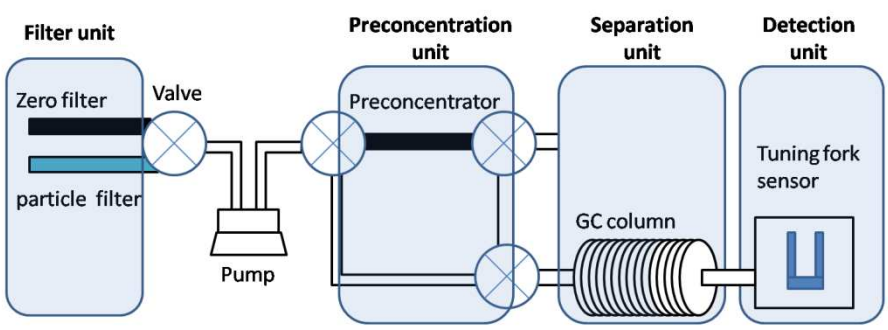

(b)

Figure. 2-1. (a) Schematic representation of the hybrid device. (b) The picture of the hybrid device, insert: the smartphone user interface showing a real time detection of a BTEX mixture sample.

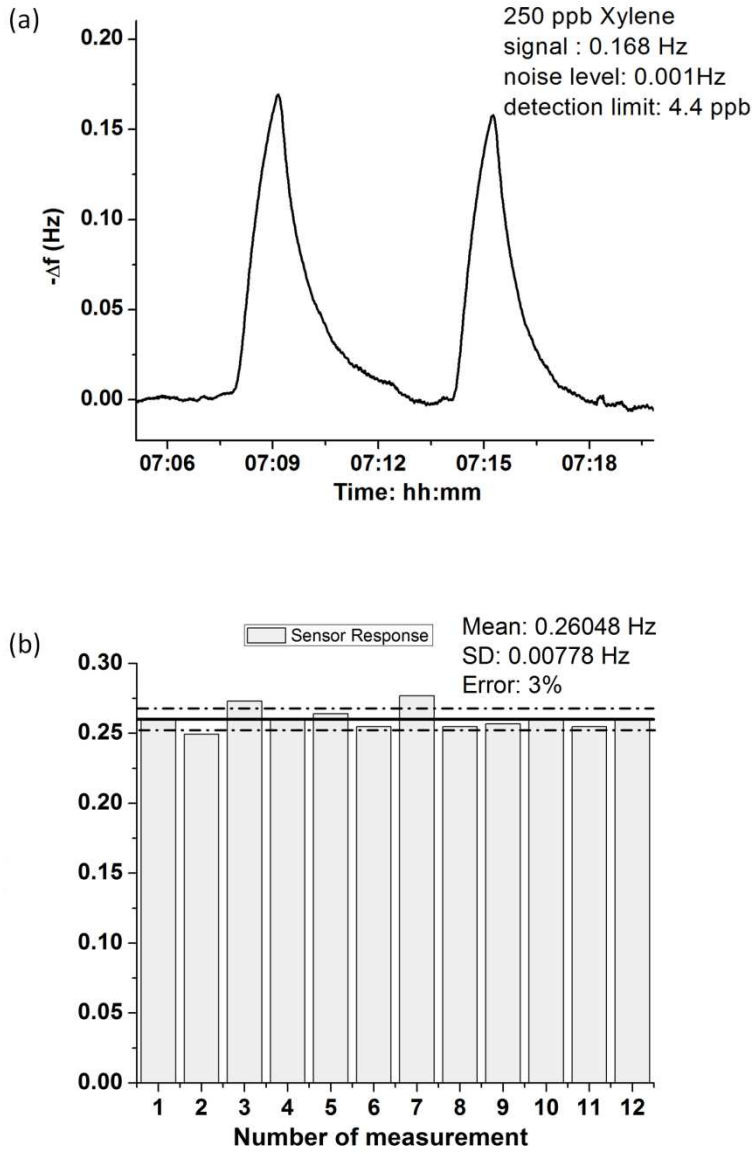

Figure. 2-2. (a) Response of tuning fork sensor to 250 ppb xylenes. Detection limit: 4.4 ppb xylenes. (b) Results of 12 measurements of the same xylenes sample using the tuning fork sensor.

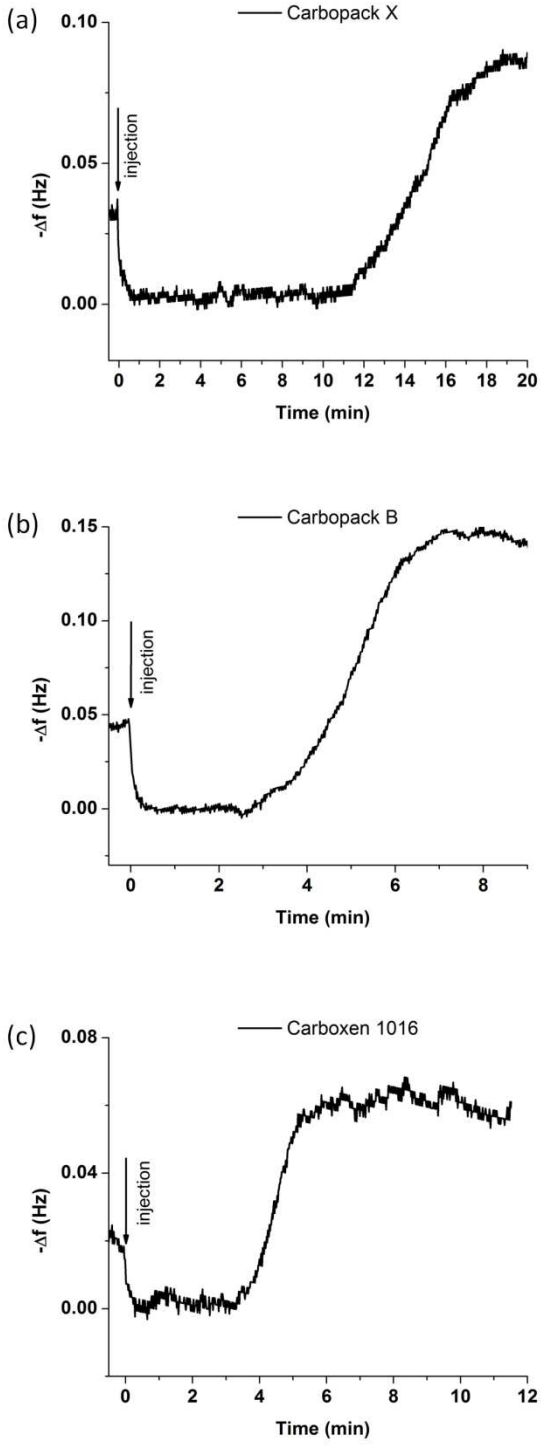

Figure. 2-3. The breakthrough time tests of three different adsorbents: (a) Carbopack X, (b) Cabopack B, (c) Carboxen 1016.

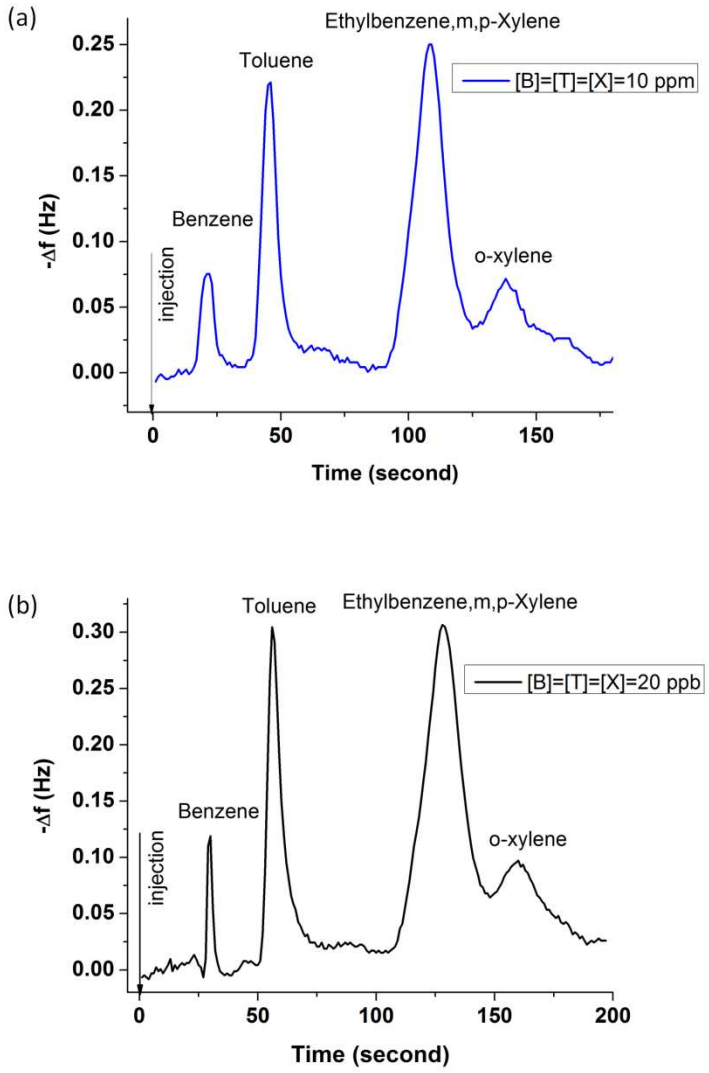

Figure. 2-4. Chromatograms of BTEX sample with and without preconcentration.

(a) BTEX sample direct injection without preconcentration, concentration:

10 ppm. (b) BTEX sample injection with 20 minutes preconcentration time, concentration: 20 ppb.

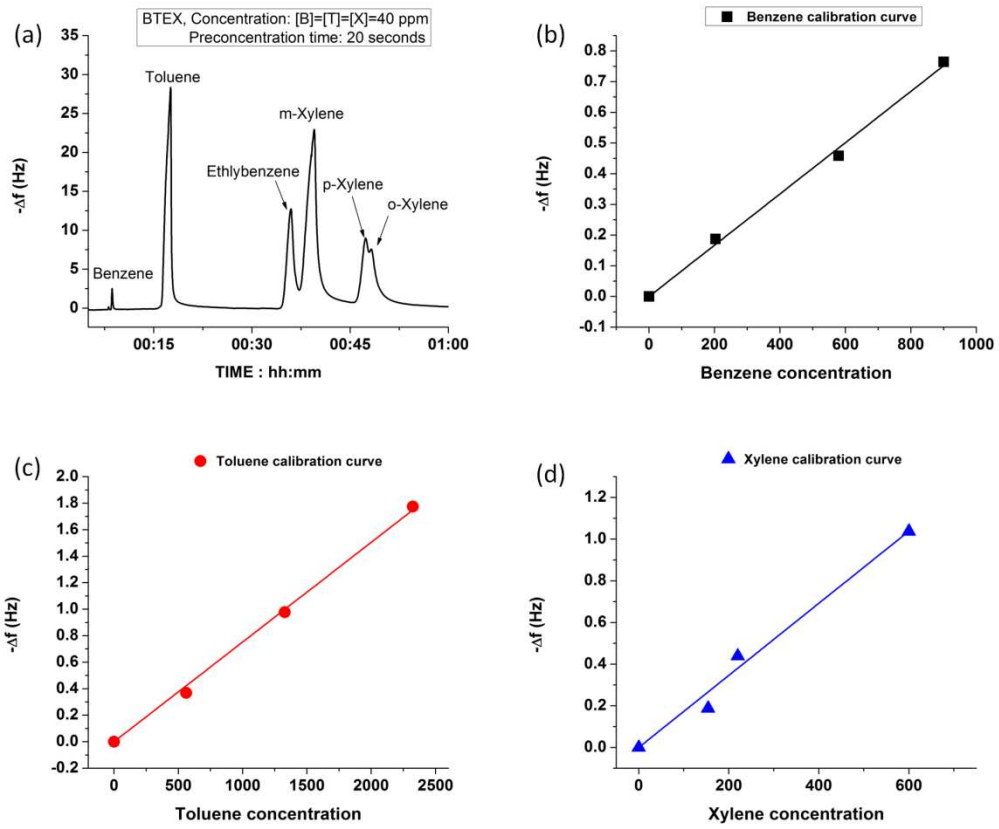

Figure. 2-5. (a) Separation chromatogram of BTEX mixtures with a 19 meters column [B] is benzene, [T] is toluene, and [X] is Ethylbenzene plus xylenes. (b), (c) and (d) are the calibration curves for benzene, toluene and xylene, respectively.

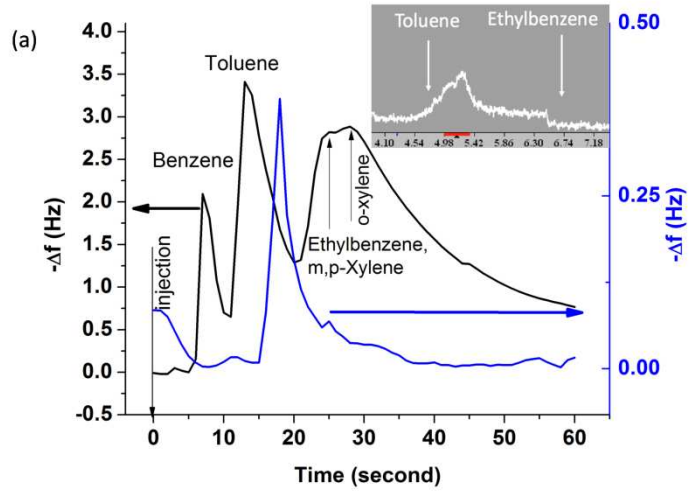

Figure. 2-6. (a) The testing result of gulf coast (blue line), the typical response of a laboratory prepared BTEX mixture (black line) and GC-MS result (insert).

(b) Map showing test location and oil spill area, date: 6-13-2010.

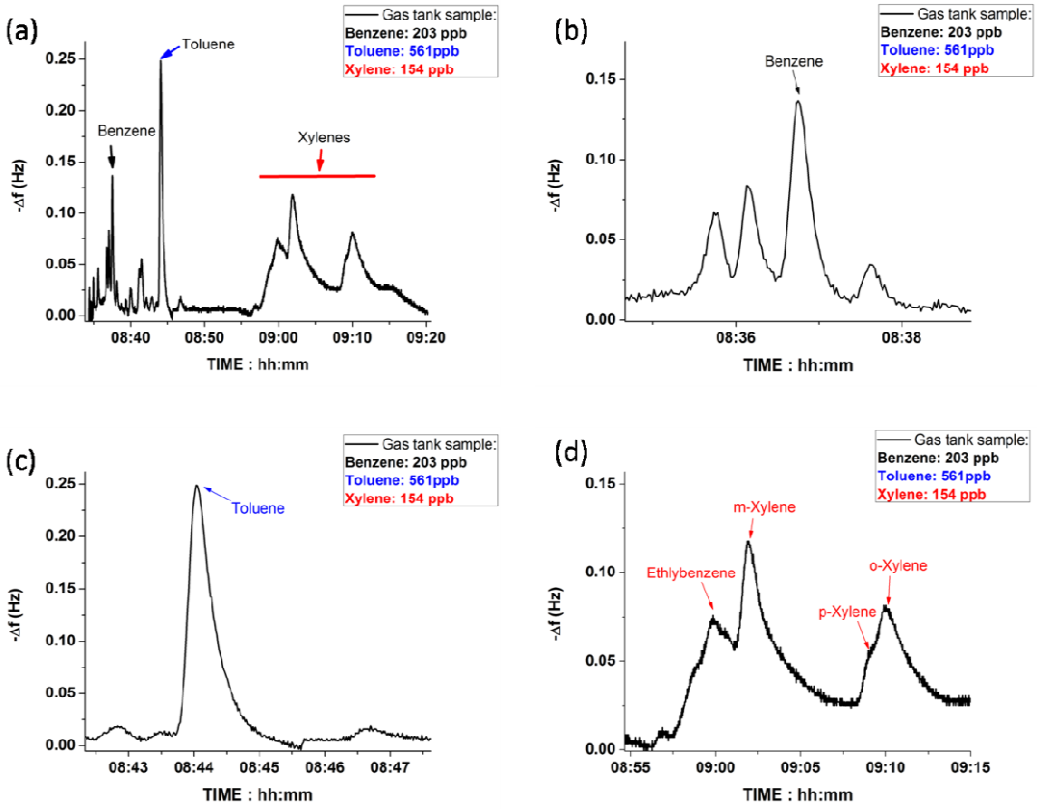

Figure. 2-7. (a) The test result of a real gasoline vapor and the corresponding detailed separation of the in BTEX compounds: (b) benzene, (c) toluene, and (d) Ethylbenzene and xylenes.

2.5 References

[1] de Medeiros, A. P. P.; Gouveia, N.; Machado, R. P. P.; de Souza, M. R.; Alencar, G. P.; Novaes, H. M. D.; de Almeida, M. F., Traffic-Related Air Pollution and Perinatal Mortality: A Case Control Study. Environmental Health Perspectives 2009, 117, (1), 127-132.

[2] Fondelli, M. C.; Bauazzano, P.; Grechi, D.; Gorini, G.; Miligi, L.; Marchese, G.; Cenni, I.; Scala, D.; Chellini, E.; Costantini, A. S., Benzene exposure in a sample of population residing in a district of Florence, Italy. Science Of The Total Environment 2008, 392, (1), 41-49.

[3] Han, X. L.; Naeher, L. P., A review of traffic-related air pollution exposure assessment studies in the developing world. Environment International 2006, 32, (1), 106-120.

[4] Harrison, R. M.; Leung, P. L.; Somervaille, L.; Smith, R.; Gilman, E., Analysis of incidence of childhood cancer in the West Midlands of the United Kingdom in relation to proximity to main roads and petrol stations. Occupational And Environmental Medicine 1999, 56, (11), 774-780.

[5] Raaschou-Nielsen, O.; Reynolds, P., Air pollution and childhood cancer: A review of the epidemiological literature. International Journal Of Cancer 2006, 118, (12), 2920-2929.

[6] Tsai, S.; Weng, H.; Yang, C., Association of Childhood Leukemia with Residential Exposure to Petrochemical Air Pollution in Taiwan. Epidemiology 2008, 19, (6), S292-S292.

[7] Weng, H. H.; Tsai, S. S.; Chiu, H. F.; Wu, T. N.; Yang, C. Y., Childhood Leukemia and Traffic Air Pollution in Taiwan: Petrol Station Density as an Indicator. Journal Of Toxicology And Environmental Health-Part A-Current Issues 2009, 72, (2), 83-87.

[8] Whitworth, K. W.; Symanski, E.; Coker, A. L., Childhood Lymphohematopoietic Cancer Incidence and Hazardous Air Pollutants in Southeast Texas, 1995-2004. Environmental Health Perspectives 2008, 116, (11), 1576-1580.

[9] Infante-Rivard, C., Chemical risk factors and childhood leukaemia: a review of recent studies dagger. Radiation Protection Dosimetry 2008, 132, (2), 220-227.

[10] Buczynska, A. J.; Krata, A.; Stranger, M.; Godoi, A. F. L.; Kontozova-Deutsch, V.; Bencs, L.; Naveau, I.; Roekens, E.; Van Grieken, R., Atmospheric BTEX-concentrations in an area with intensive street traffic. Atmospheric Environment 2009, 43, (2), 311-318.

[11] Ablat, H.; Yimit, A.; Mahmut, M.; Itoh, K., Nafion film/K+-exchanged glass optical waveguide sensor for BTX detection. Analytical Chemistry 2008, 80, (20), 7678-7683.

[12] www.defiant-tech.com

[13] www.slsmt.com

[14] www.c2v.nl

[15] www.hnu.com

[16] www.photovac.com

[17] Chia-Jung, L.; Steinecker, W. H.; Tian, W. C.; Oborny, M. C.; Nichols, J. M.; Agah, M.; Potkay, J. A.; Chan, H. K. L.; Driscoll, J.; Sacks, R. D.; Wise, K. D.; Pangad, S. W.; Zellers, E. T. Lab Chip 2005, 5, 1123–1131.

[18] Zhong, Q.; Steinecker, W. H.; Zellers, E. T. Analyst 2009, 134, 283.

[19] Zampolli, S.; Elmi, I.; Sturmann, J.; Nicoletti, S.; Dori, L.; Cardinali, C. Sens. Actuators, B: Chem. 2005, 105, 400–406.

[20] Zampolli, S.; Elmi, I.; Mancarella, F.; Betti, P.; Dalcanale, E.; Cardinali, . C.; Severi, M. Sens. Actuators, B 2009, 141, 322.

[21] Iglesias, R.; Tsow, F.; Wang, R.; Forzani, E.S.; Tao, N.J.; Anal. Chem. 2009, 81(21)8930-8935.

[22] Ren, M. H.; Forzani, E. S.; Tao, N. J. Anal. Chem. 2005, 77, 2700–2707.

[23] Tsow, F.; Forzani, E. S.; Tao, N. J. Anal. Chem. 2008, 80, 606–611.

[24] Tsow, F.; Tao, N. Appl. Phys. Lett. 2007, 90, 174102.

[25] Ren, M. H.; Tsow, T.; Forzani, E. S.; Tao, N. J. Abstr. Pap. Am. Chem. Soc. 2005, 229, 396-ANYL.

[26] Negi, I.; Tsow, F.; Tanwar, K.; Zhang, L.; Iglesias RA.; Chen, C.; Rai, A.; Forzani, ES.; Tao, N.; "Novel monitor paradigm for real-time exposure assessment", Journal of Exposure Science and Environmental Epidemiology, jes.2010.35.

[27] Solomon, G.; Janssen, S.; JAMA, 2010, Vol 304, No. 10, 1118-1119.

[28] Ellman, M.; Navarr O, K.; Solomon, G.; Environ. Sci. Technol. 2010, 44, 8365–8366.

[29] Sacks, R.; Klemp, M.; Akard, M. Field Anal. Chem. Technol. 1996, 1, 97–102.

CHAPTER 3

A PERSONAL EXPOSURE ASSESSMENT SYSTEM FOR CHEMICAL TOXICANTS

Abstract

An innovative device set, including a wearable volatile organic compounds (VOC) sensor and a docking station with gas chromatograph (GC) capability is described. Both devices employ a novel molecularly imprinted polymer (MIP) modified tuning fork VOC sensor. The wearable VOC sensor detects the total VOC concentration, it also includes a preconcentrator to absorb the VOC. This sensor can be plugged into the docking station, where a detailed GC analysis can be done. A smartphone with Bluetooth is used for data receiving, processing and storage. Data is plotted on the smartphone screen and the user can control the device from the phone also. Various key hardware components are discussed, laboratory characterization of both devices are presented and two field testing are conducted.

3.1 Introduction

Toxic volatile organic compounds (VOCs), including aromatic and chlorinated hydrocarbons, have serious environmental and health impacts [1]-[2], but they are often used in large quantities [1]-[2]. A group of VOCs including benzene, toluene, ethyl benzene and xylenes, collectively known as BTEX, are of great concern of many epidemiologists. The main source of BTEX emissions (more than 80 percent) are automobile exhaust and other traffic related sources [3]-[5]. These VOCs are defined as class A pollutants by US Environmental Protection Agency (EPA) because they are potential carcinogens, and many cause leukemia, lymphomas and other diseases [6]-[13].

Precise identification of the VOCs remains a challenge. The health effects of pollutants may vary depending on the genes of the individuals and on acute vs. accumulated exposure levels. These facts and considerations underscore the important of a wearable device that can provide both in real-time and accumulated exposure levels of individuals. The device mush be also low cost and user friendly in order to have a real impact on large population studies.

Electrochemical sensors are usually commercialized as convenient portable gas monitors, their target analytes include oxygen, carbon monoxide, hydrogen sulfide and sulfur dioxide [14]-[15]. However, these sensors are not able to detect the BTEX. Different detection methods combine with gas chromatograph (GC) is another approach. These detection methods include thermal conductivity (TCD) [16], photoionization (PID) [17]-[18], flame ionization (FID) [17], electrochemical [14], [19], and surface acoustic wave (SAW) sensors [20]. Micro machined columns and preconcentrators have been integrated with SAW and chemresistor detectors [21]. Portable GCs offer great capability

and flexibility for epidemiological, environmental and safety applications. However, the micro fabricated GCs are still under development phase and the cost of tiny components seems to be higher than conventional parts. Commercially available GCs are still expensive, range from several to tens of thousands dollars), and not suitable for epidemiological studies.

Several years ago, we reported on a first generation wearable VOC device [22]. Our sensor device employs novel design polymer coated tuning fork sensors. These tuning forks are commercially available at a very low price (~ US$0.01/each). The device was capable of detecting ppb level VOCs [22]. In addition, a hybrid VOCs detector with GC capability was also reported [23]-[24], which adds GC and preconcentration to the original designed VOC device.

The device set described here includes a wearable VOC device and a hybrid docking station with GC capability. Both units use the novel tuning fork sensor which is highly sensitive and selective to VOCs. The wearable unit is able to output the total VOCs concentration results, and the docking station will provides a detailed chemical discrimination and speciation of VOCs. This chapter provides a complete characterization of the device set with a few field testing examples.

3.2 Prototype Description and Experimental Methods

3.2.1 Prototype features and operation modes overview

Figure 3-1 presents the overall view of the wearable VOC device and hybrid docking station device set. Figure 3-2(a) and (b) shows the schematic of the wearable

VOC device and hybrid docking station, respectively. And Figure 3-2(c) shows the schematic when the two are combined.

The wearable VOC device is essentially the same as the wearable unit being developed by us in previous project [22], [25]-[26]. To briefly summary, it used quartz crystal tuning fork as a sensor [22], [25]-[26], which is coated with a layer of molecularly imprinted polymer (MIP). The MIP is synthesized in the lab using DVB as monomer and cross-linker, xylene as template and AZBN as initiator.

The wearable VOC device is powered with one 2200 mAh battery (6050100, Tenergy) and one 1000 mAh battery (PRT-00339, Unionforture Electronic Co, Ltd), it has two modes: purging and sampling. Under purging period, air is drawn by the on-board miniature diaphragm pump (135 FZ-LC, Schwarzer Precision) through an zero filter at a flowrate about 400 mL/min, the tuning fork sensor is being cleaned during this time and the VOCs inside chamber or bonded to the sensor are blown away, replaced by clean air. After two minutes of purging, the miniature 3-way latch valve (LHLA_11211H, The Lee Company) then switch from the zero filter to a particle fiber made of polyester fiber for one minute. This filter will stop the particles but let the VOCs through, during this time, the air is drawn into the sensor chamber, and the VOCs molecular will bond onto the MIP coated on the sensor.

The quartz tuning fork (CFS145-32.768KDZF-UB, CITIZEN AMERICA) has its oscillation frequency at 32.768 KHz with a very high Q factor (up to 10,000) [22]. After coated with MIP, the oscillation frequency will shift downwards, and the Q factor will also decrease because of the mass loading [22]. The sensor is then employed in the wearable VOC device. Its oscillation frequency will decrease upon the absorption of the

VOC molecular. The circuit inside the device performs the function of frequency counting. The raw data is then sent to the on-board Bluetooth (RN-41, Roving Networks Inc.), which can be paired with a smartphone with Bluetooth capability, and with the VOCs application installed in it. In this project, we use a Motorola Q9h smartphone, it runs on Windows Mobile 6 operation system. The raw signal, which is the frequency shift during a sampling period, is proportional to the concentration of injected VOCs. The calibration, which will be discussed later, will give relationship between the VOCs concentration and the raw frequency shift. The calibration factors are then stored in phone, for the VOC application to calculate the VOCs concentration when given the raw frequency shift data.

However, a critical difference between the wearable VOC device in this project versus the previous one is that, is contains also a preconcentration component that collects analytes. The preconcentration unit is located in serial with the zero filter, but closer to the air inlet. So during the purging period, when air is drawn through the zero filter, it went through the preconcentration unit first. The preconcentrator unit is a stainless steel tube filled with preconcentration materials, which is a graphitized carbon black (corbopack X, Simga-Aldrich). The preconcentrator unit will trap the VOCs molecular, but it will not interfere with the normal operation of the wearable VOC device because it is placed in the purging channel, which is supposed to remove the VOCs from the air.

An additional particle filter is placed in front of the preconcentrator to protect it from contamination, and two addiction valves are used, with one between the extra particle filter and the preconcentrator, the other one between the preconcentrator unit and

the zero filter. Both of valves have their common port connected to the preconcentrator, then the extra ports connect to flow plug 1 and 2, respectively. The preconcentrator is wrapped with a heating wire along with a thermistor, both buried in a layer of heat conductive electrically insulation coating. An electrical plug that contains the pins for the two valves, thermistor and heating wire is also included in the new unit.

At the end of each day, the user plugs the wearable device into the hybrid docking station much like a battery charger, and the device operates in the “sleep” mode.

The docking station contains a zero filter, a flow pump, two valves, a gas chromatography column, control circuit, Bluetooth chip, and a tuning fork sensor sitting inside a chamber with very small dead volume. It also includes two flow plugs and one electrical plug receptor, all in corresponding to the ones on the wearable device, as shown in Figure 3-1 and Figure 3-2.

Once the wearable is plug into the docking station, the two pairs of flow plugs conduct and the because of the electrical plug, the two extra valves inside the wearable device are now under control of the docking station.

The docking station now analyze the VOCs that trapped in the preconcentrator. There are three different flow paths and four operation modes during this measurement, as shown in Figure 3-3. The analyze starts with mode 1, sample releasing. During this mode, the preconcentrator is heated up to 300 °C, by turning on and off the heater (the heating wire) based on the temperature measurement feedback from the thermistor. The absorbed VOCs will be released from the preconcentrator material but trapped inside the preconcentrator tube in gas phase. This mode lasts for 1 minute, in the meantime, the

pump purges clean air to the sensor chamber through the GC column, and the sensor establishes its baseline during this period.

The docking station then enters operation mode 2, sampling injection. As shown in Figure 3-3(b), the pump purges the preconcentrator with clean air, carry all the released gas phase VOCs into the GC column. This sample injection mode will last for 15 seconds, which is sufficient to purge the released VOC vapor into the inlet of the GC column.

Operation mode 3, shown in Figure 3-3(c), is called analysis mode, since the VOCs vapor is also injected into the GC column, scrubbed clean will be drawn to continuously carry the vapor through the GC column. The analytes will be separated while travelling through the GC column, and enter the sensor chamber at different elution time, cause the tuning fork sensor to show corresponding responses. The tuning fork sensor is exactly the same kind as in the wearable VOC device.

The duration of operation mode 3 will vary depends on the flow rate and column length of the system. There are two different column lengths we have implemented into the system, 2 meters column and 19 meters column, for different analyte complexities. And because of the very small inner diameter of the column, elution times for the same analyte is much longer in 19 meters column than in 2 meters column.

After the analysis mode is done, the docking station enters the cleaning mode. In this mode shown in Figure 3-3(d), the preconcentrator will be heated to 300 °C, and clean air is drawn to purge the preconcentrator to remove analyte residues. The preconcentrator is then regenerated and ready for next sampling.

The docking station uses the same tuning fork sensor as in the wearable VOC device, so same frequency counting circuit was used, and the raw frequency data is sent to a smartphone via Bluetooth for processing and storage.

3.2.2 The preconcentrator in the wearable device

The preconcentrator traps the VOCs analyte and release them upon high temperature. Its housing material is very critical; it needs to have good heat conductivity and a low thermal mass, so it can be heat up quickly and uniformly. It also need to be chemically inert and stable under high temperature (up to 300 °C), and mechanically strong. All these requirements are met by stainless steel tube. A large tube would increase the thermal mass and introduce some unnecessary dead volume, on the other hand, if the stainless steel tube diameter is too small, the flow rate of the system would be restrained. We found a diameter of 1/8 inch wells served our purpose.

The preconcentrator material is a very important component, it need to be able to efficiently collect the low concentration targeted molecular, like benzene or toluene, while avoid absorbing other high concentration interferents like alcohol or ketones. Commercially available absorbent materials have been reviewed (table 1) and several of them have been chosen for further studies due to the great capability of absorbing VOCs, these are Carbopack X, Carbopack B and Carboxen 1016 from Simga-Aldrich [23]-[24].

Carbopack B and Carbopack X are graphitized carbon blacks; Carbopack B is non-porous while Carbopack X is porous. Carboxen 1016 is carbon molecular sieve which is the carbon skeletal framework remaining after the pyrolysis of a polymer precursor. The absorption capacity, release efficiency have been compared and

Carbopack X had the best performance. The breakthrough volume tests were also carried out and the mass of the chosen absorbent, which was Carbopack X, was decided to be 12 mg, which will fit into a 5.5-cm length stainless steel tube with the 1/8 inch mentioned above. The 12 mg Carbopack X was placed in the middle of tube, and was confined with two plugs of glass fiber that will prevent the material from leaking out.

During the normal operation of wearable device, the preconcentrator material Carbopack X absorbs the VOCs. When the wearable unit is plugged onto the docking station, it will be heated to 300 Celsius in order to release the absorbed analyte. A Joule effect heater is employed for providing heat. First, a layer of ceramic coating is applied on the surface of stainless steel tube as an electrically insulation and heat conductive layer. Then a nichrome wire is wrapping around the stainless steel tube. The length of the wire was optimized. If it was too long, the resistance would be proportionally big, and the heating power, which is reversely proportional to the resistance, will be reduced. However, if it was too short, then the wrapping density on the tube would be reduced, and the uniformity of the heating cannot be guaranteed. A final length of 30 cm is chosen, and the resistance is about 15 ohms. Lastly, another ceramic coating is applied on the nichrome wire to help the heat spreading, and a thermistor is also buried in this coating. Upon heating, a DC 12 voltage is applied to the wire, providing about 9.6 watts heating power. The resistance of the thermistor (10M5321, Honeywell Sensing and Control) will change when the temperature changes. The actual resistance of the thermistor is measured by the circuit, and is converted into temperature by the microcontroller. The same microcontroller then sends a control signal to turn on and off the heater based on that information.

3.2.3 Fabrication and optimization of the GC components of the docking station

Several GC columns with different stationary phase are compared. For the purpose of hydrocarbon VOCs separation, especially the separation of BTEX group, a column with cyanopropylphenyl stationary phase gave the best performance. Besides the stationary phase, the diameter and the length of the column are also essential to its performance. Usually small diameter column is preferred because the analyte interact more with the stationary phase. However, in a portable GC system, smaller diameter means increased flow resistance, which may not be feasible for a miniature pump that is usually employed in such a system. The length of the column needs optimization, as well. Longer column will usually provide better separation, but the peak broadening may increase as well. Again for such a portable GC system, where the pressure that the pump can provide is limited, longer column will decrease the flow rate and increase the analysis time. The carrier gas flow rate will affect the column separation performance. The best flow rate for a given column is given by Van Deemter equation. However in a portable system, the available miniature pump determine the highest available flow rate. Among the commercially available low noise and small size pumps, we found that a diaphragm pump (T3EP-1ST-05-3FFP, Parker) suits our needs best. The optimal diameter we chose is 0.25 mm. During the study, two different column lengths are tested. One is 2 meters and the other is 19 meters. The 2 meters column will provide a super-fast measurement of a benzene, toluene, ethyl benzene and xylenes (BTEX) mixture with acceptable separation; while the 19 meters column will provide a superior separation over the BTEX mixture, at the cost of the much longer duration.

3.2.4 The flow plug between the wearable device and docking station

The flow plug between the wearable device and the docking station makes it possible for the docking station to analyze the VOCs trapped in the preconcentrator, which is located inside the wearable unit. This flow connector needs to have a very small volume to avoid sample dilution. It also has to be strong, inert and air tight when plugged in. At the same time, to be user friendly, it has to be easy to plug in and plug out. Teflon tubes are used for this purpose. As shown in Figure 3-4, Teflon tube A's outer diameter is 1/4 inch, and the inner diameter is 1/8 inch; Teflon tube B's outer diameter is 1/8 inch and inner diameter is 1/16 inch; Teflon tube C's outer and inner diameters are 1/16 inch and 1/83 inch, respectively. When Teflon tube C is inserted into Teflon tube B, it fills the inner volume of tube B, and the combination effectively becomes another Teflon D with outer diameter 1/8 inch and inner diameter 1/83 inch. Notice that now when Teflon tube D is inserted into Teflon tube A, it fills the inner volume of tube A, and leaves very small volume inside. In practice, Teflon tube D is placed in the docking station, and Teflon tube A is inside the wearable device. The inlet of tube A is tapered so that the two parts can be relatively easy plugged in and out, but still with excellent sealing. The dead volume introduced from the connector is almost negligible because of the extremely small tube diameter.

3.2.5 Zero filters and particle filters

As shown in Figure 3-2, the wearable device contains two particle filters and one zero filter; and the docking station contains one zero filter.

The zero filter is made of 120 mg activated carbon (Purakol Media, Purafil) and 220 mg of potassium permanganate (Odoroxidant SP Media, Purafil), both in 12/16 mesh. These two are used in combination for broad-spectrum pollutant removal. At the inlet and outlet of the filter, there is also a polyester fiber plug, to prevent the materials from moving, and also serving the purpose of filtering the incoming particles. All these material are placed into a 15 cm long Teflon tube with 1/16 inch inner diameter. The particle filter is simply made of 30 mg polyester fiber contained in the same type of tube mentioned above.

3.2.6 The user interface on a smartphone

Powerful smartphones are now widely available, they not only have great computing power, but also have many peripherals that can be very useful for a person monitor [27]-[29]. For example, the light intensity sensor in a phone can indicate whether the person is indoor or outdoor; the accelerometer will give information regarding a person's activity; and a GPS chip makes it easy to record the location of events.

As shown in Figure 3-1, we created two applications for the two units on the Motorola Q9h smartphone, which contains a Bluetooth and GPS chip. The application (app) can establish a wireless connection with the devices through Bluetooth. The device then sends the raw data of the tuning fork sensors and the valve status to the smartphone. The app then process the data, apply the factors and display the results on the screen.

For the wearable unit, the app display the most recent 3 minutes of real time reading of the sensor, which is updated every second. The user can also switch the view to concentration plot, where the concentration data is shown, and is updated every 3

minutes. Besides the two graphs, the app also shows the current time, the current operation mode, the temperature measured by the circuit, the sensor working status, and the GPS location data. The left function key lets the user choose which tuning fork sensor in the sensor array will be shown on the screen, as well as the option to switch between real time data plot and concentration plot as mentioned above. The right function key offers the GPS on/off option, and also allow the user to apply different calibration factor to the results, this calibration factor will be discussed in detail later. Raw data as well as the concentration data will be saved on phone, the user can also exit the app through the right function key menu.

The phone application for the docking station has some differences compared with the one for the wearable unit. After this app established a Bluetooth connection with the docking station, the docking station is in stand-by mode. The user then has two options: define the individual duration for the sample releasing mode, analysis mode and the cleaning mode and then start the measurement, or just start the measurement using the default duration values for those modes. Once the measurement starts, the real time reading of the tuning fork sensor is plotted on the screen, updated every second. The current time and current mode information are also shown. Raw data will be saved on the phone, and the user is able to exit the app through the right function key menu.

3.3 Results and Discussion

3.3.1 The wearable VOC device operation

The operation of our previous generations of wearable VOC devices is briefly described in the introduction part of this thesis. A more detailed description is given below.

As mentioned before, this wearable unit is essentially the same as the previous VOC device with a few more components, and it will function like a normal VOC device [22], [25]-[26] by itself. The interior of this unit is shown in Figure 3-5. It contains one particle filter and one zero filter, one miniature diaphragm pump, one latch valve, control circuit, Bluetooth chip, tuning fork sensor and chamber, a nafion tube, one battery with 2200 mAh capacity, another battery with 1000 mAh capacity and several flow connection components. These are the essential parts of a wearable VOC device. In addition, one particle filter, one preconcentrator, two latch valves, two flow connector and one electrical connector are included in this unit as well, so that it can preconcentrate the VOCs during its normal sampling, and work with the docking station for a more precious analysis.

Upon turning on, the wearable unit turns on the circuit, Bluetooth, the pump and the valve. The device starts with purging mode (Figure 3-6(a)), the pump draws air through the zero filter, cleans the tuning fork sensor and establish a baseline for the sensor. This mode lasts for 2 minutes. Notice that the preconcentrator also collects sample during this period. The valve then switches to the particle filter channel, and this is so called sampling mode (Figure 3-6(b)). The sample air is drawn into the sensor chamber, causing the tuning fork sensor response.

The wearable unit was calibrated using o-xylene. Figure 3-6(c) shows the tuning fork response to 1 ppm (parts per million) xylene. The 2 minutes purging and 1 minute sampling cycle was repeated automatically, the signal is taken from the frequency change during the 1 minute sampling period. Notice that the frequency change is negative upon sampling, due to the adding mass to the tuning fork sensor.

3.3.2 The wearable device validation using selected-ion flow-tube mass spectrometry

As mentioned above, once the calibration factor was found, we can measure unknown sample using the raw sensor response and the obtained factor. The accuracy of the device is evaluated using a selected-ion flow-tube mass spectrometry (SIFT-MS).

The sensor's calibration factor was determined prior to this test. During the validation, four Tedlar sample bags contain different unknown concentrations of o-xylene were created. Each of them was then sampled by the device as well as the SIFT-MS. Figure 3-7(a) shows the device readings plotted against the values of the SIFT-MS. Notice there were two tuning fork sensors in the sensor chamber. When putting two sensors in one device, in case one sensor stopped functioning, the other will still be able to output measurement results. And extra sensor data also offers more data processing possibilities.

Figure 3-7(b) shows the correlation between the average of the two sensors readings and the SIFT-MS readings. The value of R-square is 0.99619, indicates a very good correlation.

3.3.3 Temperature effect on the sensor response

When temperature increases, the kinetic energy of the VOCs molecular will also increase. And because of that, upon equilibrium, less VOCs molecular will bond on the molecularly imprinted polymer coating on the tuning fork sensor, resulting in a smaller response, thus a lower sensitivity.

To investigate the temperature effect on the sensor response, we tested four different environmental temperatures besides the room temperature, which is 25 °C. In each test, the device and the VOCs gas sample were kept in a refrigerator or an oven for half an hour so that they can reach the equilibrium temperature. Then the measurement starts, and the sensor responses and the environmental temperature were recorded.

Figure 3-8 shows how the sensitivity decrease when the temperature increase. The y axis is the relative sensitivity at that temperature compared to the sensitivity at 25 °C. The 0.97444 R-square value indicates a pretty good linearity for this relationship. And a -0.03944 slope shows that with every increasing °C from 25 °C, the sensitivity would drop 3.944%.

When the temperature coefficient of the sensor was determined in this method, it then can be used for temperature compensation of the device results. There was a temperature sensor inside the device which reports the temperature reading to the microcontroller, and the information was then sent the application on the smartphone. The temperature coefficient was implemented in the phone application and the compensation was automatically done.

3.3.4 The Operation of the Hybrid Docking Station

The interior of the hybrid docking station is shown in Figure 3-9. The major components include a miniature gas pump, two latch valves, one GC column, one zero filter, one sensor chamber with a tuning fork sensor, control circuit, Bluetooth chip, two flow plugs, and one electrical plug.

As shown in Figure 3-2(c), when the wearable device is plugged into the docking station, the two pairs of flow plugs connect and the electrical connection grants the docking station ability to control the two valves, thermistor and heater of the preconcentrator inside the wearable unit.

And then the docking station will go through the four operation modes in sequence: sample releasing, sample injection, analysis and cleaning, as shown in Figure 2-3.

The combined operation is illustrated in Figure 3-10. First, a one liter volume Tedlar bag is filled with standard 1 ppm BTEX gas sample. This sample bag is then connected to the wearable device for measurement. This measurement lasts for six minutes. As mentioned above, the device starts in purging mode, which last two minutes, then switches into sampling mode, lasts one minute. And this three-minute cycle is repeated automatically. The configuration of this test is shown in Figure 3-10(a). Also shown in Figure 3-10(a) is the tuning fork sensor response in this test. A change of 0.36 Hz of the tuning fork sensor is developed by the 1 ppm BTEX gas sample. Only one complete cycle is shown here.

Because two thirds of the time, the device is in purging mode, which means the preconcentrator is working for four minutes out of the six minutes test duration. The

wearable unit is then plugged into the docking station as shown in Figure 3-10(b). This action connects the two flow plugs and one electrical plug. As illustrated in Figure 3-3, the docking station now has control of the preconcentrator, and the hybrid docking station is now ready to analyze the trapped BTEX sample in the preconcentrator.

The analysis starts with mode 1, shown in Figure 3-3(a). In this sample releasing mode, the docking station supplies 12 V DC to the heater, quickly brings the preconcentrator to 300 °C. Once the temperature reaches 300 °C, the docking station maintains that temperature by turning on and off the heater, based on the temperature reading from the thermistor. The thermistor is a resistor that will change its resistance value when the temperature changes. A fixed value resistor is placed in serial with this thermistor, and a 3 V DC voltage is applied across this two resistors voltage divider circuit. Then the voltage V_R across the fixed value resistor is measured using the ADC (analog to digital convertor) pin on the micro controller. In this way, the resistance of the thermistor can be found using the formula below:

$$\frac{V_R}{R} = \frac{3 - V_R}{R_T}$$

In which V_R is the voltage drop on fixed resistor R = 100 ohms, and R_T is the resistance of the thermistor.

Then we substitute R_T into the formula to find T:

$$B = \frac{T_0 T}{T - T_0} \ln \frac{R_0}{R_T}$$

Where B is beta value of the thermistor, in this case, B = 3947 K. Room temperature T_0 = 298.15 K, and room temperature resistance of the thermistor R_0 = 100 K ohms.

For the purpose of saving the micro controller processing power and time, instead of calculating the temperature using the formulas above every second, and compare it with 300 °C (573.15 K), we just simply calculate the corresponding voltage V_R when T = 573.15 K. That way, we can just compare the measured voltage value V_R with $V_R(T$ = 573.15 K), and avoid all the complex calculations. A simple calculation gives the $V_R(T$ = 573.15 K) = 1.516 V.

The value of V_R is sampled every second, which is not extremely fast, there is then some overshot or drop in the temperature. When simultaneously monitored using an external thermal coupler, the steady state temperature variation is found to be ±5 °C, meaning the temperature is kept within 300 ± 5 °C, which is well acceptable for our purpose.

In general, the temperature ramps up to 300 °C in 30 seconds, and then it maintains at that 300 ± 5 °C for the remaining 30 seconds of this sample releasing mode. The heating end temperature and the heating duration determine how efficient the trapped sample will be released from the preconcentrator material to gas phase. To find the minimum required temperature, initial tests on lower temperatures are conducted. It is found that heating the preconcentrator up to 200 °C can well release benzene and toluene, but not ethyl benzene and xylenes, for which, 300 °C is required. Although these preconcentrator materials are stable to above 400 °C, for thermal desorption, the temperature is typically 330 °C [30]. So it is possible to increase the heating temperature even further. However, even though the preconcentrator tube itself is made from stainless steel, the other connections are made of Teflon, including the flow tubes and the valve. Heating at 300 °C for a minute is within but very close to the limit of these components,

going for even higher temperature may significantly degrade their quality. It is also an option to replace all these Teflon flow tubes with stainless steel tubes, that way we can employ higher temperatures. However, we still favor Teflon tubes for their flexibility, which is very important in device prototyping stage, allow us to quickly change designs.

And as shown in Figure 3-3 (a), while the preconcentrator is undergone heating, the pump draws air through the zero filter, and push it into the sensor chamber. This is very necessary to establish the sensor response baseline, because we are looking for changes in the signal once the actual analyte comes in.

At the end of the mode 1, the circuit switches the four valves to form a flow channel from the pump to the preconcentrator, then to the GC column. This is the so-called injection mode. During this mode, the pump draws clean air through the zero filter, purge through the preconcentrator and carries the released sample into the GC column. This mode lasts for 15 seconds. Upon calculation, the volume from beginning of the preconcentrator to the beginning of the GC column is around 400 µL, and the flow rate in this mode is at least 3 mL/min. ideally, it takes about 8 seconds to purge this much volume. However, to be safe and sure that the pump can bring all the sample into the GC column, 15 seconds injection time is chosen. This doubles the minimum required time and ensures that 100% of the sample is carried into the GC column. The heater tries to maintain the preconcentrator at 300 °C during this period.

When the injection ends, the valves are switched so that the device enters the analysis mode. The sample has been sent into the GC column, and in this mode, the pump draws clean air to carry the sample through the column. As the sample goes through the column, they interact with the column stationary phase. The interaction strength is

different for different components. The stronger the interaction is, the slower that component moves along the column. The component with the least interaction will come out of column first. The GC column used in this device, which is UAC-502 from QUADREX Corporation, uses volatile organics phase. The volatile organic components generally come out according to their boiling point. So in the case of BTEX sample, the order is benzene, toluene, ethyl benzene and xylenes.

As shown in Figure 3-10(b), benzene reaches the sensor chamber first (even before the injection period ends), followed by toluene and xylenes. The xylenes contains ethyl benzene, o-xylene, p-xylene and m-xylene, and that's why two peaks are seen for xylenes. The length of this column in this test is 2.5 meters. In the later chapter, we should see that when the column length is increased up to 19 meters, the separation becomes much better with the pump, ethyl benzene, m-xylene, p-xylene and o-xylene are well separated. However, the increased separation is at the cost of increasing analysis time. And if the length of the column is reduced from 2.5 meters to 2 meters, the separation performance is scarified but the analysis time becomes even shorter.

The elution time, which is the time duration from the injection to when the peak appears, is 11 seconds for benzene, 22 seconds for toluene, 55 seconds and 67 seconds for the first and second peak of xylenes.

The tuning fork sensor at the end of the GC column is the same as the one used in the wearable unit, it responds to the BTEX components and shows peaks as they arrives at the sensor chamber.

The analysis mode's duration varies depends on the length of the column. In this test, the elution time of the slowest component is 67 seconds, and the analysis time is set to be 120 seconds to make sure all analytes can exit the column.

When the analysis time is up, the device goes to into cleaning mode. As shown in Figure 3-3(d), the valves are switched so that the pump can blow air into the preconcentrator to clean it. Again the heater is turned on to release any residual analyte in the preconcentrator. This step lasts for 60 seconds. After that, the preconcentrator is refreshed and ready for next use.

The data is saved on the smartphone by the application. Every second one piece of data is added into a text file. Each piece contains the current date and time, the sensor raw reading and the valve status (mode status). The real time plot is shown on the smartphone. The data file can be downloaded into a computer for further analysis.

Based on the elution time information, one is able to identify the individual component of a VOC mixture. The following section describe the calibration of the docking station device under different column length configurations.

3.3.5 The Calibration of the Hybrid Docking Station

With the elution time information, we can identify the individual component of a VOC mixture. To accurately know the concentration of each component, the docking station needs to be calibrated.

To calibrate the device, known concentration of BTEX are prepared. First, 40 ppm BTEX is prepared using a 40 L Tedlar sample bag. Then a 50 mL syringe is used to transfer some of the 40 ppm BTEX gas to another 40 L Tedlar sample bag. If we take 50

mL, then the final concentration in the other bag will be 50 ppb because of the dilution. The reason that the low ppb BTEX sample is not prepared directly is that it's difficult to make sure the accuracy because of the extremely low BTEX liquid amount needed. For example, to prepare a 40 ppb BTEX sample using a 40 L Tedlar bag, one needs to put 6.32 nL benzene, 7.52 nL toluene and 9.04 nL xylene into the bag, which is very hard to measure and transfer accurately. However, preparing a 40 ppm BTEX sample then needs 6.32 µL benzene, 7.52 µL toluene and 9.04 µL xylene, which is much easier to archive. For this reason, we choose to dilute a high concentration sample to get a low concentration sample.

Once the known concentration BTEX sample is prepared, it is sampled by the wearable unit for a fixed amount of time, and the preconcentration time is then calculated as two third of the sampling time of the wearable unit. After the preconcentration is done, the wearable unit is then plugged into the docking station for analysis.

The first column configuration is 2.5 meters. Figure 3-11 shows the results of docking station analysis when the wearable unit is used to preconcentrate 50 ppb, 30 ppb and 10 ppb BTEX for 9 minutes. The first peak belongs to benzene, the second is due to toluene and the last one peak with a shoulder is because of the ethyl benzene and xylenes can't be fully resolved. Notice the sensor response to benzene is the smallest and that to xylenes is the largest, a result of the different sensitivity of the sensor to different VOCs.

Figure 3-12 shows the calibration curve for benzene, toluene and xylene. Notice for xylenes, only the first peak is taken into account. The slope is 0.0147 Hz/ppb for benzene, 0.0385 Hz/ppb for toluene and 0.0766 Hz/ppb for xylenes. The sensitivity ratio is about 19: 50: 100 for benzene: toluene: xylene.

As mentioned above, for the 2.5 meters column, the elution time is 11 seconds for benzene, 22 seconds for toluene, 55 seconds and 67 seconds for the first and the shoulder of xylenes.

The second column configuration is 2 meters. For a shorter column, one can expect poorer separation performance but faster analysis time. Figure 3-13 shows the results of the docking station for 50 ppb, 25 ppb and 10 ppb BTEX sample that is preconcentrated by the wearable unit for 10 minutes. Notice that the shoulder that can be seen in the previous test disappears, ethyl benzene, o-xylene, p-xylene and m-xylene now all converge into one peak, an indication of the poor separation performance. The elution time in this configuration is 6 seconds for benzene, 13 seconds for toluene and 32 seconds for xylenes. These values are about 50% less than that in the 2.5 meters configuration. So this configuration can be used for ultra-fast analysis with acceptable separation performance, because benzene, toluene and xylenes are still well separated.

Figure 3-14 shows the calibration curve for this configuration. The slope is 0.01981 Hz/ppb for benzene, 0.0373 Hz/ppb for toluene and 0.05305 Hz/ppb for xylene. Compare this result with the previous one, the slope for benzene and toluene are similar, but not for xylene. And the reason could be due to converge of the two peaks lower the overall peak height.

The last column configuration uses a 19 meters long column. This column provides the best separation but at the cost of an extremely long analysis time. This configuration can be very be useful when analyzing a complex VOC mixture.

Figure 3-15 shows the results of the docking station analyze 25 ppb and 10 ppb BTEX sample that is preconcentrated by the wearable unit for 30 minutes. Notice for

these tests, there are drifts at the first part of the curves, from 0 to about 12 minutes. Also there is an unknown disturbance to the sensor at around 12 minutes which is not due to the analyte.

The elution time is around 5 minutes for benzene, 14 minutes for toluene, 31 minutes for ethyl benzene, 34 minutes for m-xylene and 43 minutes for p-xylene and o-xylene, which is extremely long compared to the previous configurations, but with superb separation performance. Once the device is calibrated, it can be used on field to test real samples. Two examples are given below.

3.3.6 Field tests of the device

The first field test samples the lab air and office air at Biodesign institute, Arizona State University. Both areas are non-smoke, well ventilated. At each place, the wearable unit samples the air for 6 hours, which means a 4 hours preconcentration time. It is then plugged into the docking station for analysis. 2.5 meters column length configuration is used in this test.

Figure 3-16 shows the results of the office air and lab air, along with a standard 1 ppm BTEX sample. It shows that no benzene is found in either place. However, a tiny amount of toluene and xylene are found in these two samples. At the same time, there is one unknown peak appears between benzene and toluene, also another one between toluene and xylenes.

The concentration of the toluene is 40 ppt for office air and 100 ppt for the lab air, and the concentration of xylene is 30 ppt and 90 ppt for office air and lab air, respectively. So that although they are both very clean, the lab does contains a little bit more toluene

and xylene. Which is not surprising considering all the chemical storage and chemical experiments in the lab.

The second field test uses the 19 meters configuration. The wearable unit samples the lab air and a parking structure air for 6 hours, which again means a 4 hour preconcentration time. It is then plugged into the docking station for analysis.

The results are shown in Figure 3-17. No trace of benzene is found in either sample. There is a relatively high concentration of toluene in the parking structure air sample, but a small amount of xylenes in the same sample. These two should be due to the car exhaust and the cigarette smoke in the parking structure. The lab air result is very similar to that in the first field test, it has tiny amount of toluene and xylenes. The concentration of toluene and xylenes in the parking structure sample is calculated to be 40 ppb and 2.24 ppb, respectively; and for the lab air, they are 60 ppt and 30 ppt.

3.4 Conclusion

This study has characterized the performance of a wearable VOC device and hybrid docking station device set. The wearable unit is meant to provide real time overall VOC exposure measurement, where the hybrid docking station does a fine job in discriminate between the BTEX components and provide an extremely low detection limit. The key components of this device set are an adsorbent packed preconcentrator in the wearable unit, a GC column in the docking station and a novel tuning fork VOC detector. The tradeoffs associated with these components are illustrated. Flow plug and electrical connector are created to realize the idea of plug and play. The design criteria of these two components are also described.

In addition, two applications on smartphone are created for the two units. The application connects to the device via Bluetooth, its function includes data receiving, data storage, figure plotting and remote commanding. It can also activate the GPS function of the smartphone to enable location associated VOC exposure measurement, which can be very useful.

Different lengths of GC column are used in the docking station unit and the tradeoff between the GC separation performance and the analysis time are discussed.

Two different field tests are conducted, the high sensitivity of the device is proven to be very useful in situations where the sample are in ppt level.

However, there are still some shortcomings to address. One of the issues is the drifting of the elution time due the inconsistency of the pump and the surrounding temperature variance of the column. Some kind of flow regulator can be used to help with the pump inconsistency, and a temperature controlled enclosure for the column could solve the latter problem.

Another issue the low long-term stability of the tuning forks. This requires some insight research on the sensing fundamental of the tuning for sensor. An alternative is to design such a sensor cartridge that it can be easily replaced each time.

Table 2-1. Comparison of different adsorbent

Absorbent	Structure	Desorption Temp. (°C)	Specific surface area (m^2/g)	Cost ($) per gram
Carbopack B	Carbon black	330	100	15.5
Carbopack X	Carbon black	330	240	42
Carboxen 1016	Carbon molecular sieve	330	75	18.8
Tenax GR	Polymer	300	24	16.7
Porapak N	Polymer	180	300	5
HayeSep D	Polymer	180	795	5
Tenax TA	Polymer	350	35	14.6
XAD-4	Polymer	150	750	0.15

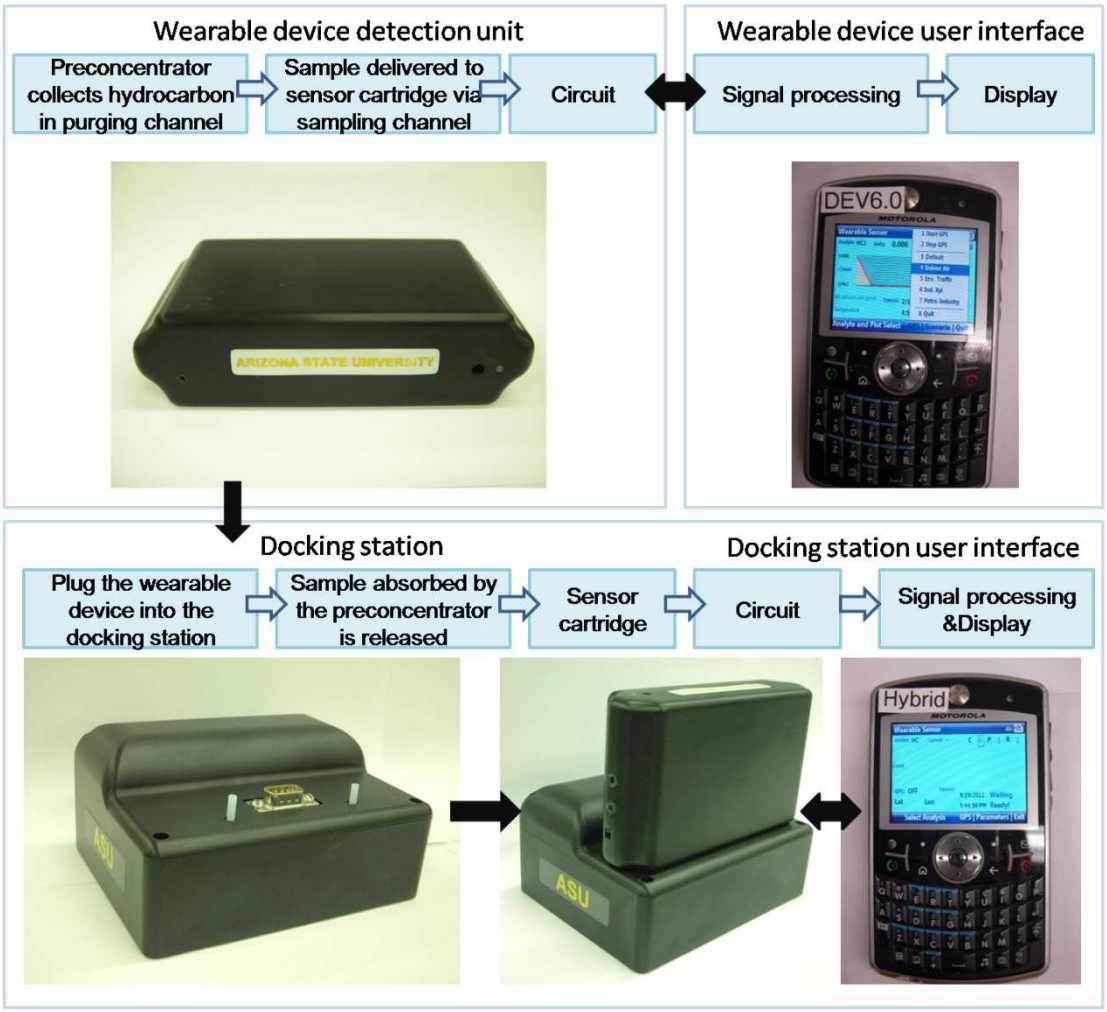

Figure 3-1. Pictures of the wearable VOC device (top left), hybrid docking station (bottom left) and their combination (bottom middle). Their corresponding applications on the smartphone are also shown. The major function of each part (device and smartphone) is shown in blue blocks.

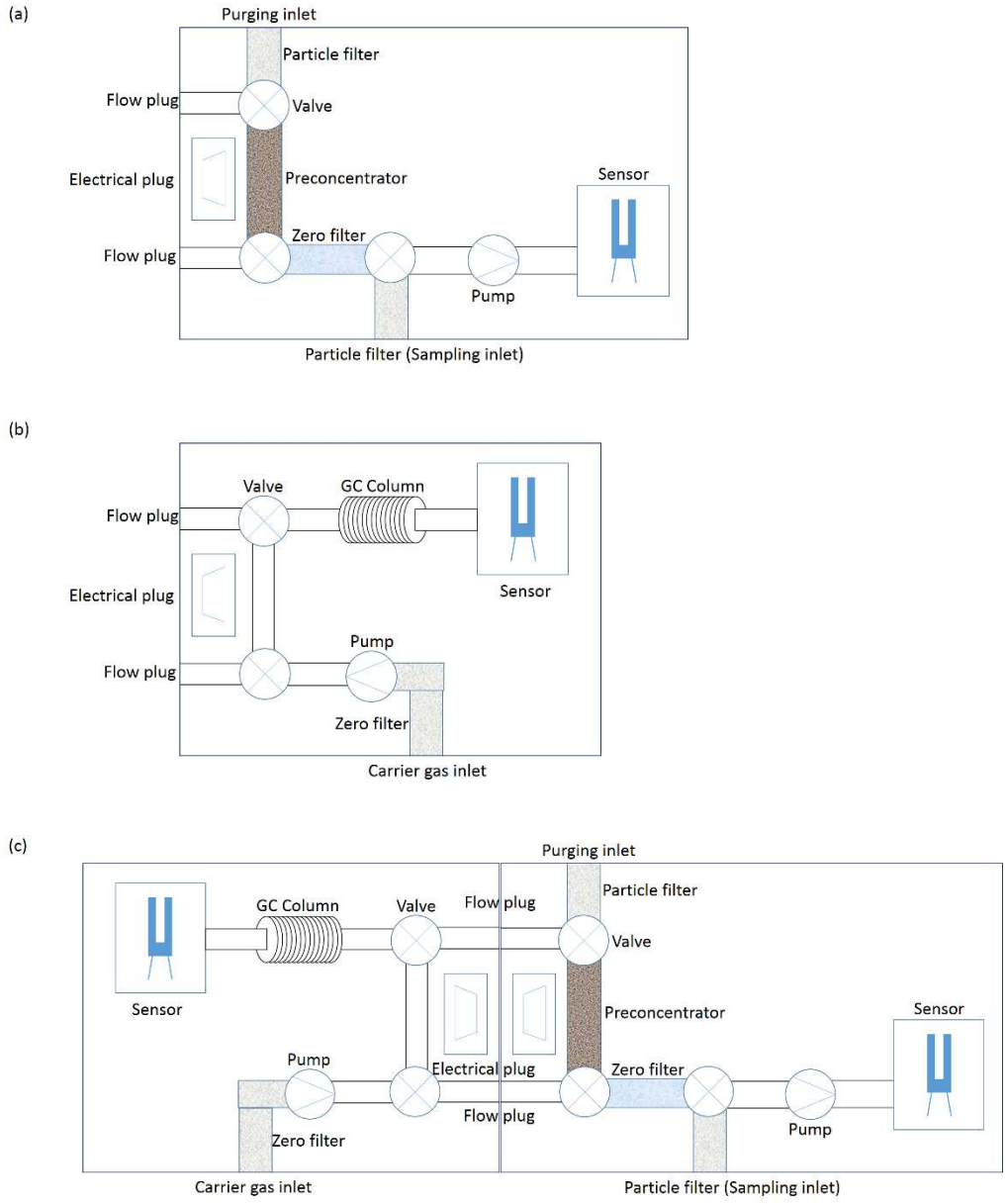

Figure 3-2. Block diagram of the devices. (a) Wearable VOC device; (b) hybrid docking station; (c) wearable VOC device plugged into the docking station.

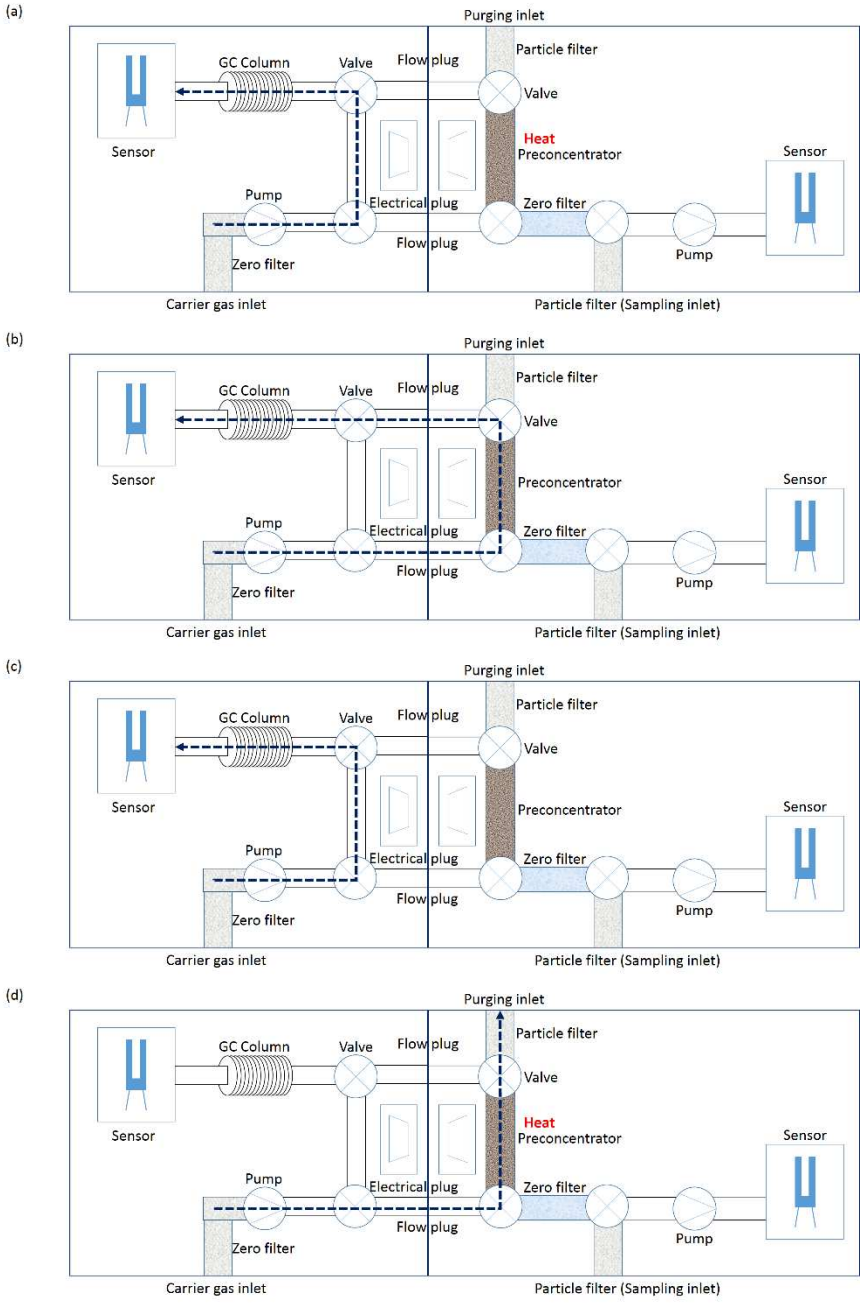

Figure 3-3. Operation modes of the device set. (a) Releasing mode; (b) Injection mode; (c) analysis mode; (d) cleaning mode.

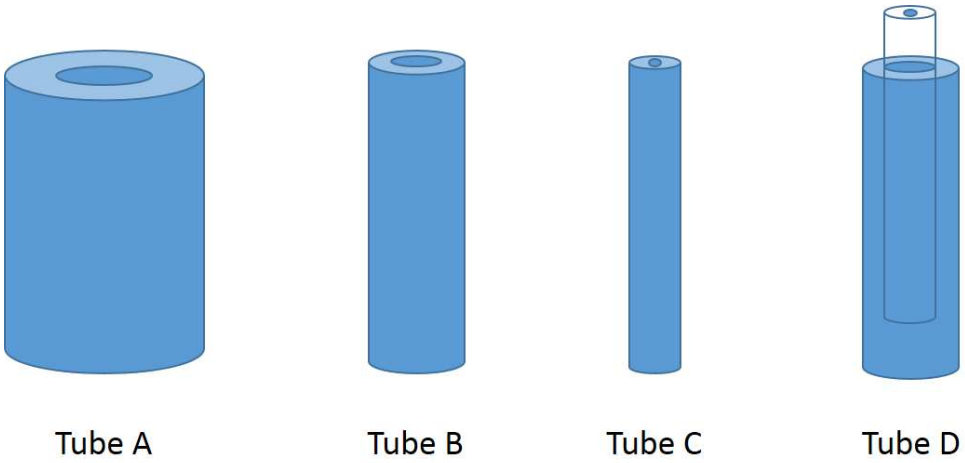

Figure 3-4. Different sizes of Teflon tubes for the flow connection between the two devices.

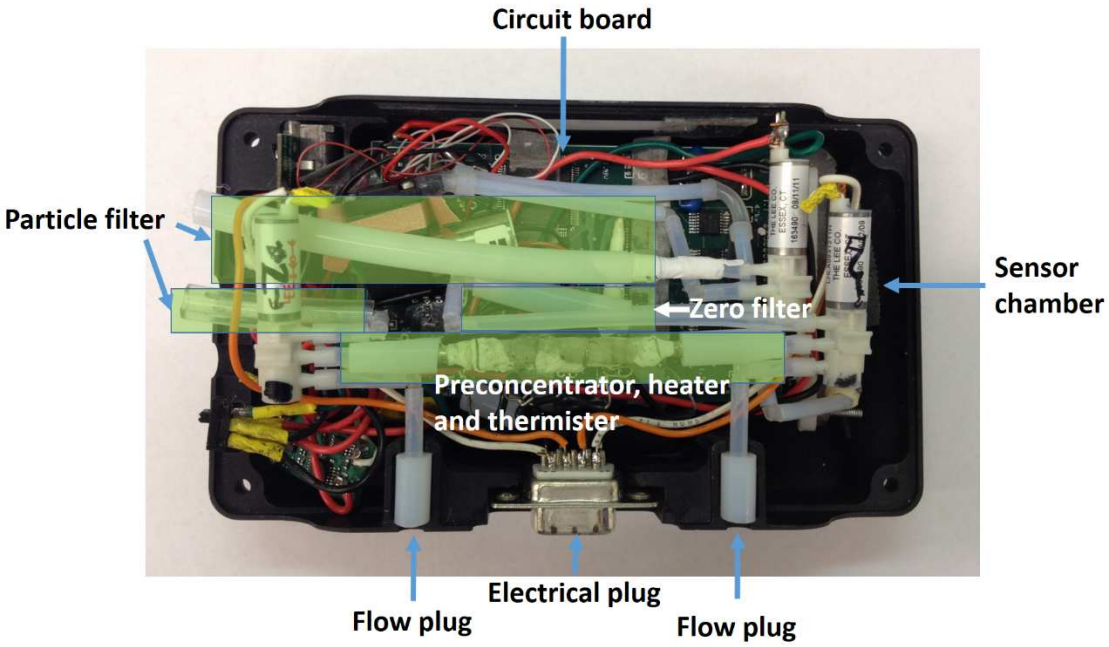

Figure 3-5. The interior of the wearable VOC device.

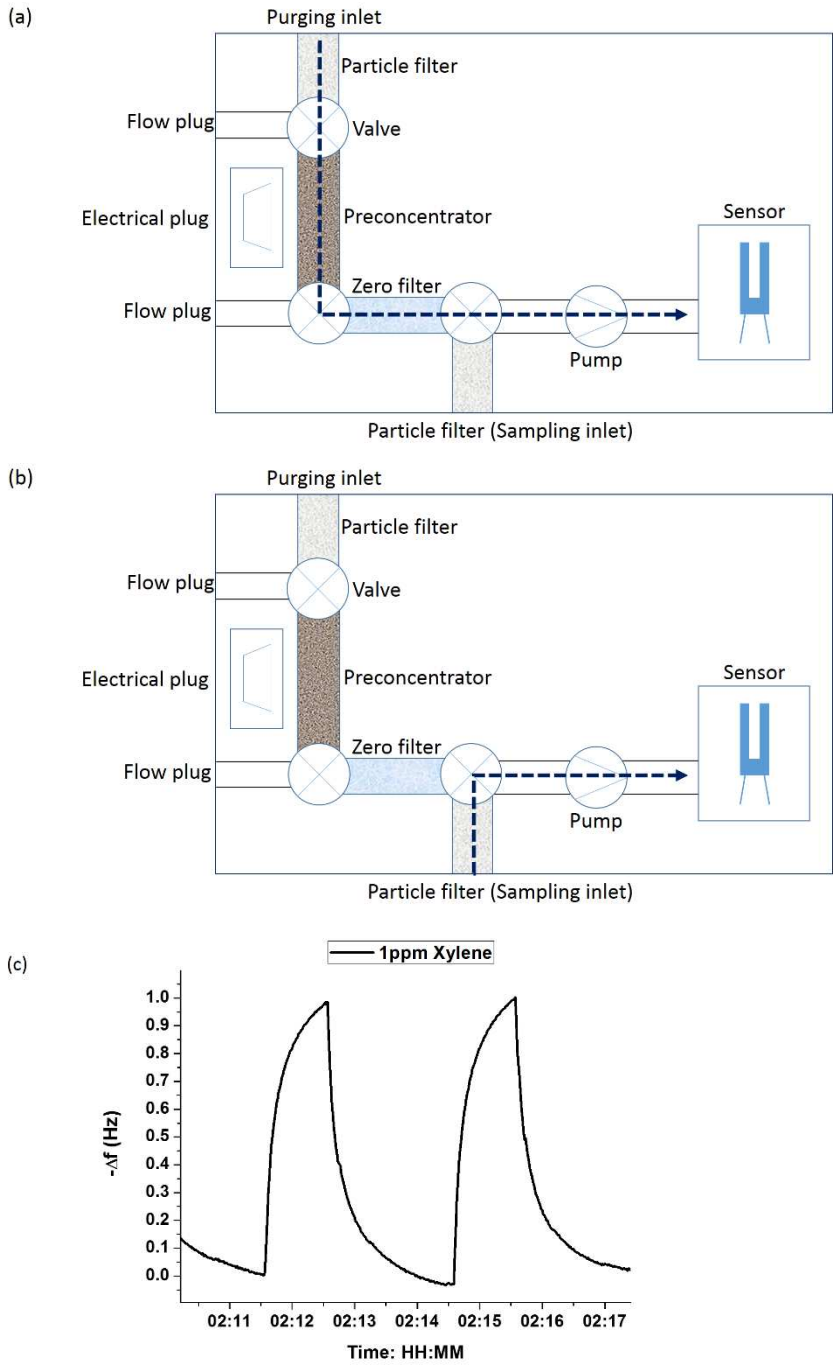

Figure 3-6. The operation modes of the wearable VOC device and the typical response. (a) Wearable device purging mode; (b) wearable device sampling mode; (c) typical response profile to 1ppm xylene.

(a)

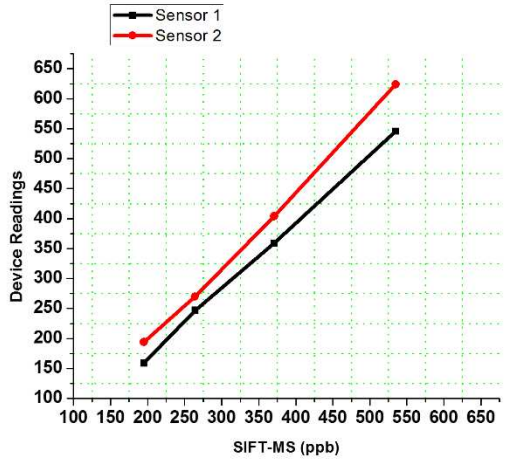

(b)

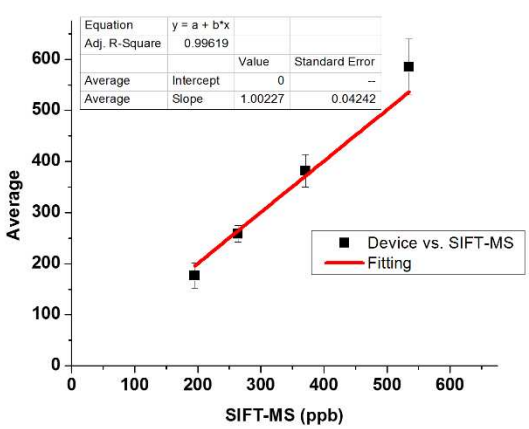

Figure 3-7. Wearable VOC device validation using SIFT-MS. (a) SIFT-MS reading vs. wearable sensor reading, for different concentrations of xylene; (b) the linear fitting of the data.

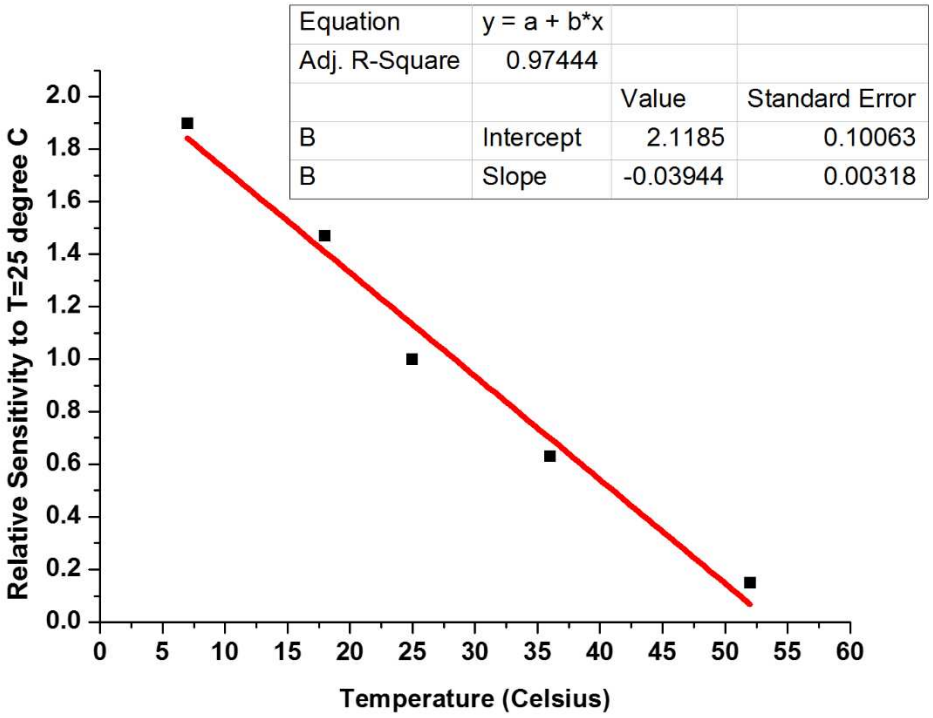

Figure 3-8. Tuning fork sensor's sensitivity vs. Temperature.

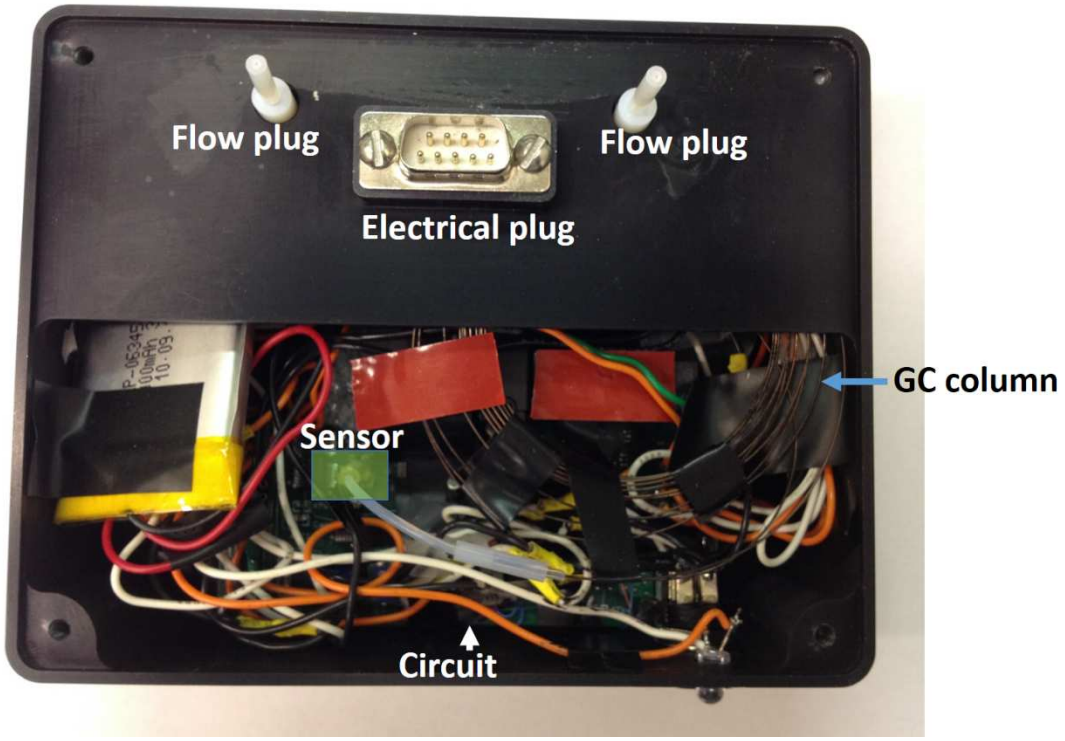

Figure 3-9. The interior of the hybrid docking station device.

(a)

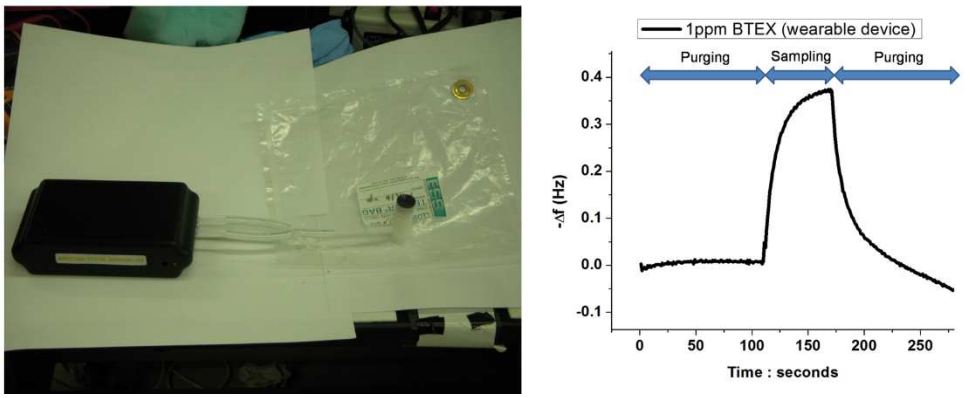

(b)

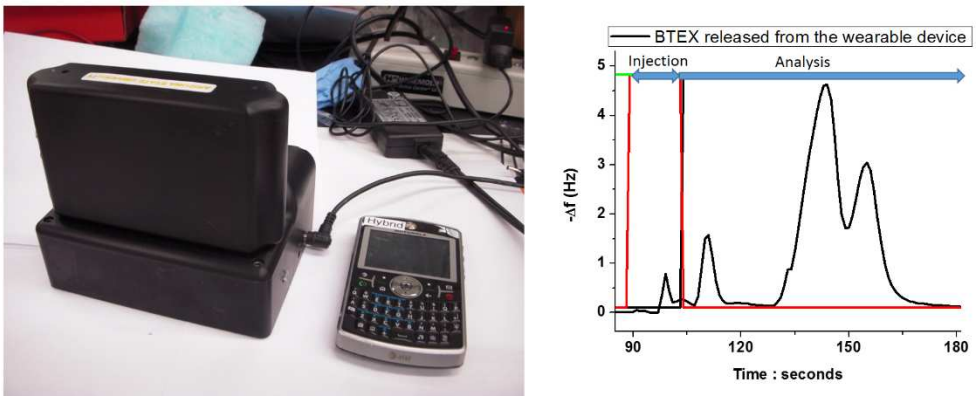

Figure 3-10. Operation of the two devices. (a) Wearable device measuring 1 ppm BTEX; (b) The docking station analyzing the preconcentrated 1 ppm BTEX.

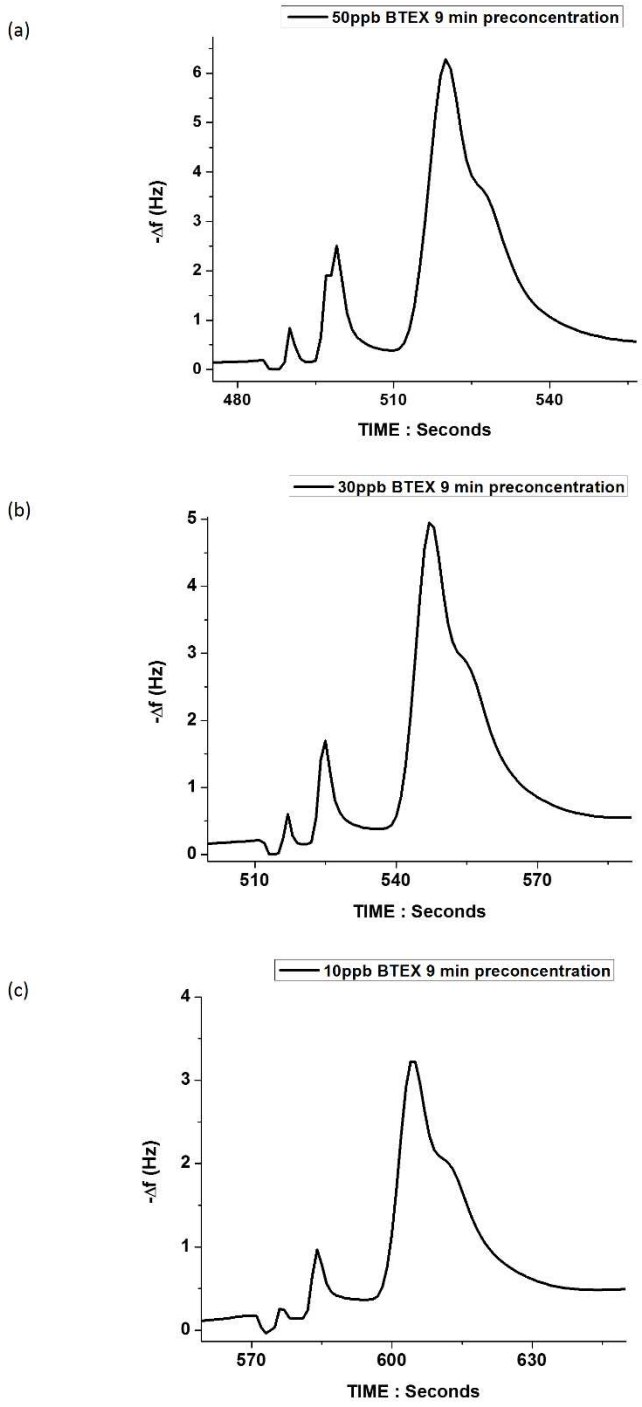

Figure 3-11. 2.5 meters column length configuration calibration. (a) 50 ppb BTEX 9 minutes preconcentration; (b) 30 ppb; (c) 10 ppb.

(a)

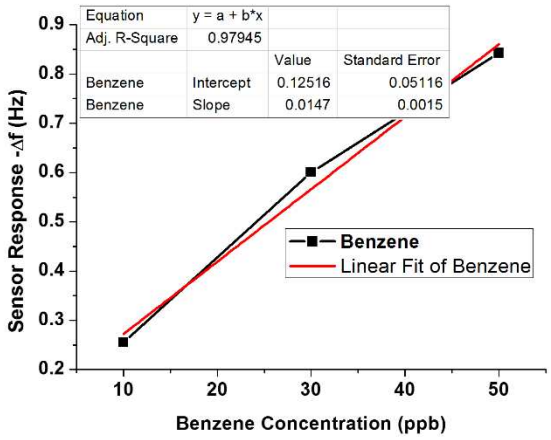

(b)

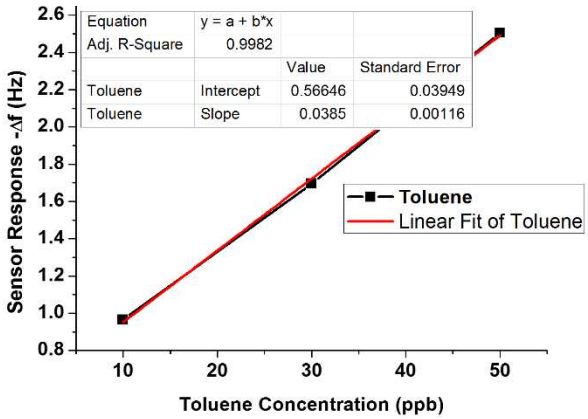

(c)

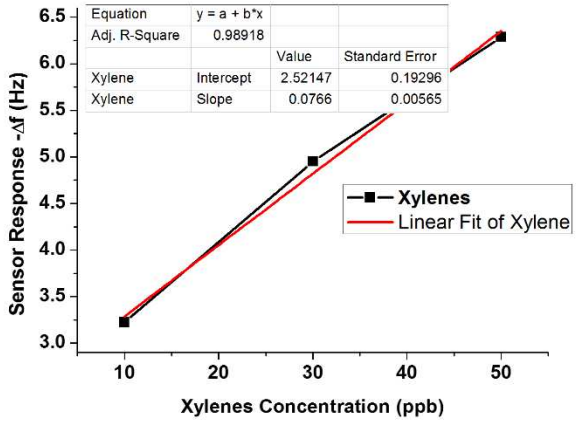

Figure 3-12. 2.5 meters column length configuration calibration. (a) Benzene; (b) toluene; (c) xylene.

(a)

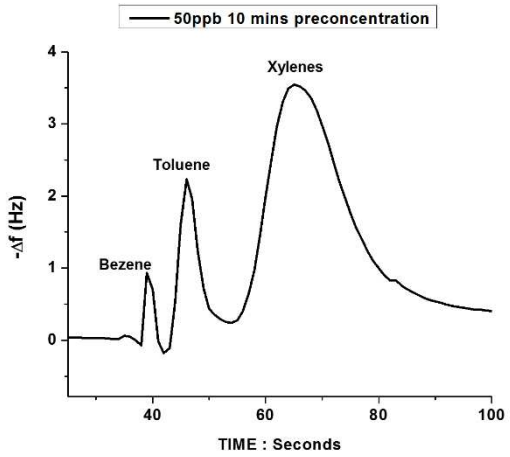

(b)

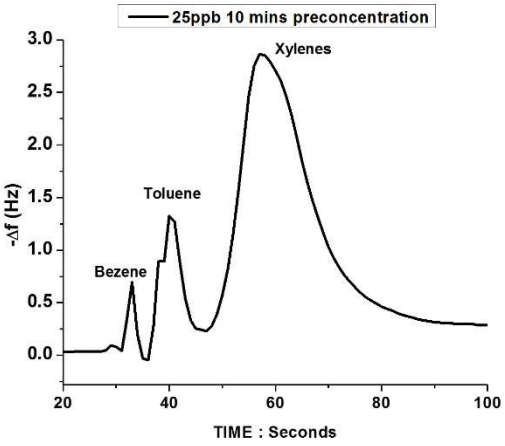

(c)

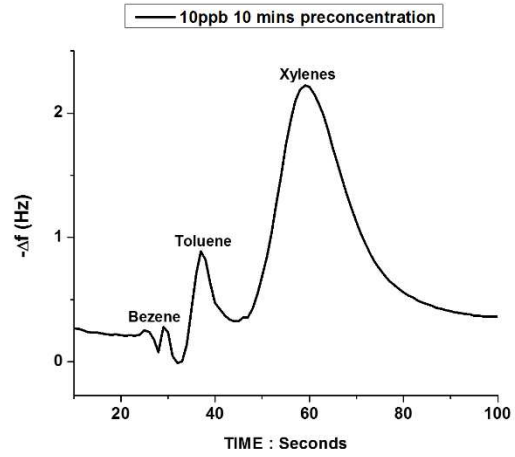

Figure 3-13. 2 meters column length configuration calibration. (a) 50 ppb BTEX 9 minutes preconcentration; (b) 25 ppb; (c) 10 ppb.

(a)

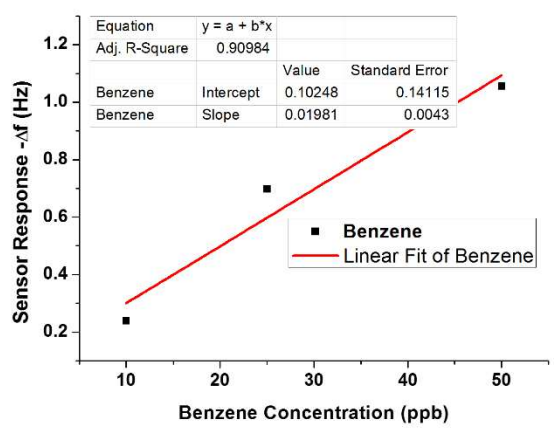

(b)

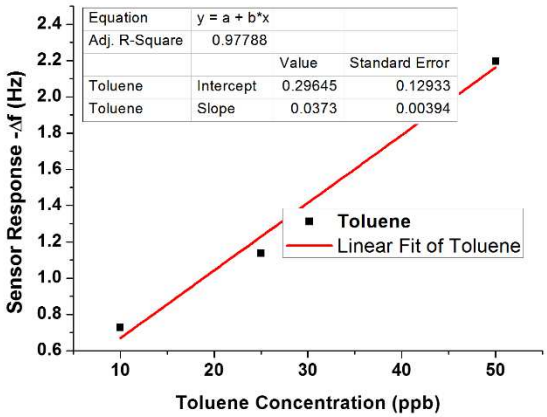

(c)

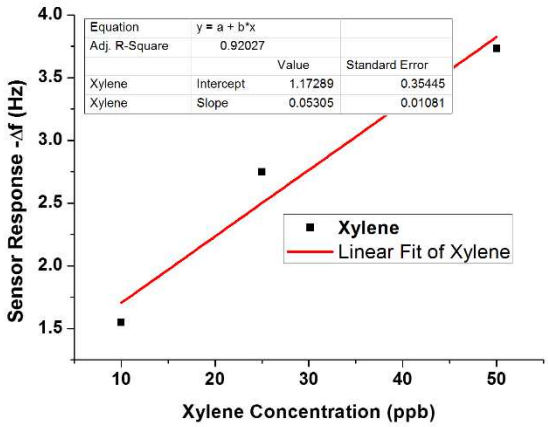

Figure 3-14. 2 meters column length configuration calibration. (a) Benzene; (b) toluene; (c) xylene.

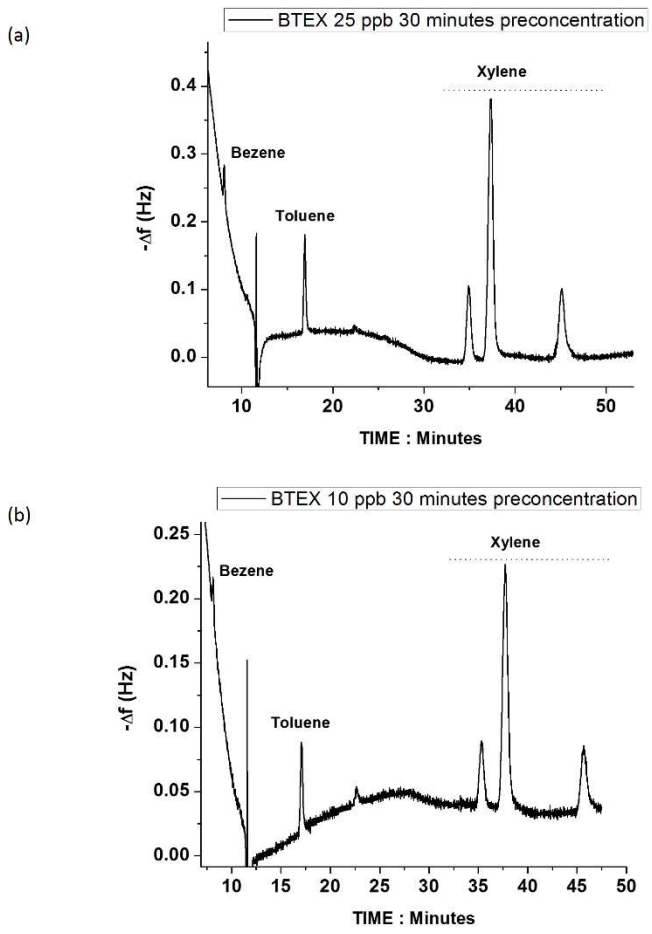

Figure 3-15. 19 meters column length configuration calibration. (a) 25 ppb; (b) 10 ppb.

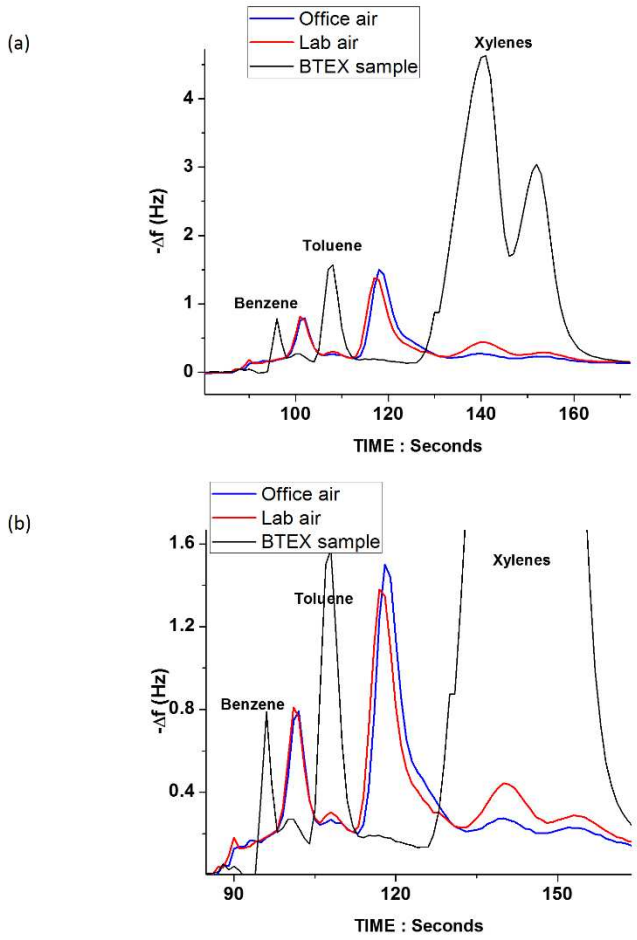

Figure 3-16. Office air and lab air compared to a BTEX sample, 2.5 meters column configuration. (a) The docking station analysis result; (b) a zoom in of (a).

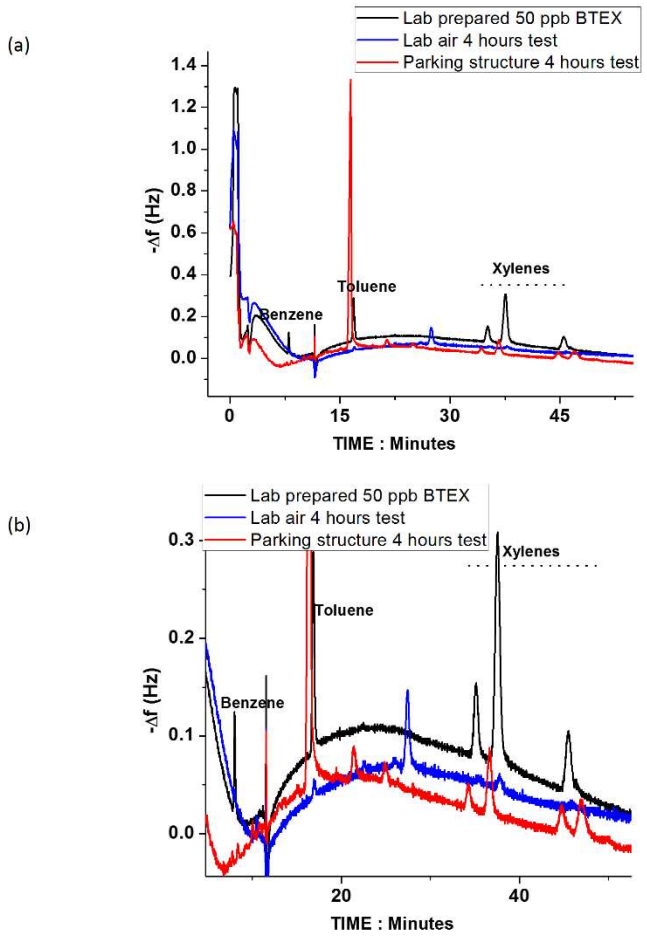

Figure 3-17. Parking structure air and lab air compared to a BTEX sample, 19 meters column configuration. (a) The docking station analysis result; (b) a zoom in of (a).

3.5 Reference

[1] Amorim, Leiliane CA, Joana P. Carneiro, and Zenilda L. Cardeal. "An optimized method for determination of benzene in exhaled air by gas chromatography–mass spectrometry using solid phase microextraction as a sampling technique." *Journal of Chromatography B* 865.1 (2008): 141-146.

[2] Sexton, Ken, et al. "Children's exposure to volatile organic compounds as determined by longitudinal measurements in blood." *Environmental health perspectives* 113.3 (2005): 342.

[3] Han, Xianglu, and Luke P. Naeher. "A review of traffic-related air pollution exposure assessment studies in the developing world." *Environment international* 32.1 (2006): 106-120.

[4] Buczynska, Anna Jolanta, et al. "Atmospheric BTEX-concentrations in an area with intensive street traffic." *Atmospheric Environment* 43.2 (2009): 311-318.

[5] Ablat, Hayrensa, et al. "Nafion film/K+-exchanged glass optical waveguide sensor for BTX detection." *Analytical chemistry* 80.20 (2008): 7678-7683.

[6] De Medeiros, A. P., et al. "Traffic-related air pollution and perinatal mortality: a case-control study." *Environ Health Perspect* 117.1 (2009): 127-132.

[7] Fondelli, M. Cristina, et al. "Benzene exposure in a sample of population residing in a district of Florence, Italy." *Science of the total environment* 392.1 (2008): 41-49.

[8] Harrison, Roy M., et al. "Analysis of incidence of childhood cancer in the West Midlands of the United Kingdom in relation to proximity to main roads and petrol stations." *Occupational and Environmental Medicine* 56.11 (1999): 774-780.

[9] Raaschou‐Nielsen, Ole, and Peggy Reynolds. "Air pollution and childhood cancer: a review of the epidemiological literature." *International journal of cancer*118.12 (2006): 2920-2929.

[10] Tsai, S., H. Weng, and C. Yang. "Association of Childhood Leukemia with Residential Exposure to Petrochemical Air Pollution in Taiwan." *Epidemiology*19.6 (2008): S292.

[11] Weng, Hsu-Huei, et al. "Childhood leukemia and traffic air pollution in Taiwan: petrol station density as an indicator." *Journal of Toxicology and Environmental Health, Part A* 72.2 (2008): 83-87.

[12] Whitworth, Kristina W., Elaine Symanski, and Ann L. Coker. "Childhood lymphohematopoietic cancer incidence and hazardous air pollutants in southeast Texas, 1995–2004." (2008).

[13] Infante-Rivard, Claire. "Chemical risk factors and childhood leukaemia: a review of recent studies†." *Radiation protection dosimetry* 132.2 (2008): 220-227.

[14] http://www.raesystems.

[15] www.draeger.com

[16] www.agilent.com/chem/microgc.

[17] www.hnu.com.

[18] www.photovac.com.

[19] http://microsensorsystems.com.

[20] http://www.estcal.com.

[21] Lu, Chia-Jung, et al. "First-generation hybrid MEMS gas chromatograph." *Lab on a Chip* 5.10 (2005): 1123-1131.

[22] Tsow, Francis, et al. "A wearable and wireless sensor system for real-time monitoring of toxic environmental volatile organic compounds." *Sensors Journal, IEEE* 9.12 (2009): 1734-1740.

[23] Iglesias, Rodrigo A., et al. "Hybrid separation and detection device for analysis of benzene, toluene, ethylbenzene, and xylenes in complex samples."*Analytical chemistry* 81.21 (2009): 8930-8935.

[24] Chen, Cheng, et al. "A wireless hybrid chemical sensor for detection of environmental volatile organic compounds." (2011): 1-1.

[25] Chen, Cheng, et al. "A new sensor for the assessment of personal exposure to volatile organic compounds." *Atmospheric environment* 54 (2012): 679-687.

[26] Negi, Indira, et al. "Novel monitor paradigm for real-time exposure assessment."*Journal of Exposure Science and Environmental Epidemiology* 21.4 (2011): 419-426.

[27] Lane, Nicholas D., et al. "BeWell: A smartphone application to monitor, model and promote wellbeing." *5th International ICST Conference on Pervasive Computing Technologies for Healthcare*. 2011.

[28] Kirwan, Morwenna, et al. "Using smartphone technology to monitor physical activity in the 10,000 Steps Program: a matched case–control trial." *Journal of medical Internet research* 14.2 (2012).

[29] Lam, Stephen Chiu Kwok, et al. "A smartphone-centric platform for personal health monitoring using wireless wearable biosensors." *Information, Communications and Signal Processing, 2009. ICICS 2009. 7th International Conference on*. IEEE, 2009.

[30] http://www.sigmaaldrich.com/catalog/product/supelco/10436?lang=en&region=US.

CHAPTER 4

A MULTI-ANALYTE COLORIMETRIC ENVIRONMENTAL SENSOR

4.1 Introduction

Monitoring of air pollutions, such as NO_2, ozone, volatile organic compounds (VOCs), is critical for environmental protection, human exposure protection and studies of different pollution related issues [1-4]. Such pollutants can cause serious health problems [5-6]. To date the most commonly used detection methods for these air pollutants is based on fixed monitoring sites using large equipment.

A low cost, small size, light weighted device that can provide fast and continuous monitoring of air pollutants is required in order to assess these pollutants with high spatial and temporal resolutions.

Colorimetric sensors detects the target analyte based on the color change upon the reaction of the sensing material and the analyte. This method is widely used for its high sensitivity and selectivity, as well as its simplicity.

Here a colorimetric device platform is presented. This device is only 120 mm long, 80 mm wide and 8 mm thick, it uses a miniature fan for the gas sample delivery. This circuit inside the device uses a high quality Sigma-Delta ADC chip to accurately measure the color change seen by the photodiode on the circuit, it also has a sensor chip that can host a colorimetric sensor that fits into its groove. The device has both wireless Bluetooth and wired cable communication interface, which will work with Bluetooth enabled android smartphone or iPhone.

This platform is tested using a NO_2 sensor to validate its capability.

4.2 Experimental

4.2.1 Platform setup

Figure 4-1 shows the schematic of the device. The sensor chip is made from a light weight, inert and transparent plastic. Up to four different sensors are placed on the sensor chip. The sensors are typically made from silicon paper coated with materials that will react with the target analytes and change colors upon reactions. On top of the sensor chip is a flat led board, which illuminates the sensor chip. There are four of same kind of photodiodes underneath the sensor chip to measure the light intensity through each sensor. On the right of the figure is a sampling fan which will deliver the environmental air into the sensor chip.

Once the sensor material reacts with its target analyte, its color will change, thus the transmitted light intensity will also change. If one of the sensor is a reference sensor, which means it is a blank silicon paper without any material coating, and we define its transmitted light intensity as I_0, and define the transmitted light intensity of a coated sensor one as I_1, then the signal we are looking for, which is the light absorbance will be:

$$A_1 = -log_{10}(\frac{I_1}{I_0})$$

The blank sensor is our reference sensor, the advantage of having this reference and calculate the absorbance is that it corrects the light source drift and environmental noise that is happening to all sensors.

The fan is controlled by a microcontroller on the device circuit. It is off for two minutes and then turned on for one minute. During the time when the fan is off, the

reaction happens very slowly, and the baseline of the absorbance is collected. Once the fan is switched on, the reaction speeds up and the absorbance change is developed.

Figure 4.2 shows the actual picture of the device. Some key components are marked on figure 4.2(a). In the middle is the sandwich configuration of the flat led board, the sensor chip and the photodiodes (underneath the sensor chip on the circuit, not shown in the picture). The sampling fan is on the bottom of the device, it draws air from top and blow it through the sensor chip. There is a LCD display chip on the top of the device, which will give indications of what the device is doing, as well as show concentration results of each measurement. This device allows for two kinds of communication: wired and wireless. The wired communication is done through the female headphone jack, where a cable can be plugged into and retrieve analyte concentration data from an iphone app. The wireless communication is realized through the Bluetooth chip. Smartphones with Bluetooth capability (right now we only support Android devices, more devices supporting are under development) can pair with the device and receive real time data from it. We offer two kinds of data retrieving methods for that each of them will become handy in certain circumstances. For example, if one just need to do a quick check up in a room, he or she can just run the device and look at the results from the LCD display, and retrieve the data from the device through a wired connection later. However, if the device needs to be placed in a remote location, then the Bluetooth communication becomes a must. All of the components are powered by a single lithium polymer battery with 800 mAh capacity, and it’s good for at least 10 hours of continues operation, and the battery can be recharged through a mini USB cable. Figure 4.2(b) shows the device with the housing. The device measures 120mm*80mm, and the thickness is only 8 mm. The LCD

is displaying “TESTING” which means the device is in the middle of a measurement, and it will show the results after the testing is done. Next to the LCD display is the switch, and the inlet of the device is on the bottom. The sensor chip is plugged through a hole on the left side of the device.

4.2.2 The photodiode measuring circuit.

The core part of the device circuit is the photodiode measuring circuit. The quality of this measurement directly effects our signal quality. The schematic of this circuit is shown in Figure 4.3(a). In this configuration, the non-inverting terminal of the operation amplifier (opamp) is connected to the ground, the cathode of the photodiode is connected to the inverting terminal of the opamp, and a feedback resistor and capacitor is connected between the inverting terminal and the output of the opamp. The output voltage will be:

$$\text{Vout} = I_D * R$$

I_D is the photo induced current, and R is the feedback resistor. This output voltage is then fed into the ADC pin of the microcontroller. The first generation microcontroller we use is from Texas Instrument (TI), model MSP430F5438A, which has a 12-bit SAR (successive approximation) ADC.

Figure 4.3(b) show typical results of photodiodes readings from this microcontroller. It can be seen that the curve is not smooth, it has a lot of steps, or in other words, repeated values in the result. And this problem of repeated ADC readings become more severe when the readings are near the 1.5 V mark. This repeated value results are not acceptable in our application, it largely increase the effective noise level of the signal and makes it difficult for ppb level detection.

The SAR ADC uses a capacitive network to digitalize the analog voltage value, and reference we use for the ADC is 3 V. So the ADC first compare the input voltage to 3/2 V, which is 1.5 V, and if the input voltage is larger than 1.5 V, the most significant bit is set to be 1. Continue the comparison for 12 times and we get a 12 bits number. The most possible reason for the repeated 1.5 V value is that is wrongly set the most significant bit to be 1, and causing the rest of bits to be 0.

Because of this significant problem associated with this ADC module, another kind of ADC, which is Sigma-Delta ADC is picked for experiment. The Sigma-Delta ADC uses a technique called oversampling to achieve high resolution ADC results. It usually provides higher resolution results than the SAR ADC, but with lower data sampling frequency. However, for our application, the data rate provided by the Sigma-Delta ADC is more than enough.

Figure 4.4(a) shows that a Sigma-Delta ADC experimental board is used to measure the photodiode readings from our device. Figure 4.4(b) shows the measurement results. It's easy to see that results are much smoother that previous ADC, and the repeated value problem is gone.

A replacement microcontroller from TI called MSP430F4794 has four channels of Sigma-Delta ADC, and also has all the peripherals that the previous microcontroller has, so the effects of adapting to this new chip is minimal.

Figure 4.4(c) shows the new schematic of the device, the only change is the new microcontroller. Figure 4.5(a) and 4.5(b) show the photodiodes measurements from the new microcontroller. Figure 4.5(c) is a zoom-in of the figure 4.5(b) to show the noise. As we can see, the noise level is about 0.1 mV, which is very low. Notice that there is a big

dip and recovery in the readings, and it is caused by the fan turning on and off, not due to the chemical reaction. Ideally, this change should behave in the same manner on both photodiodes, and therefore, with the absorbance calculation, the reference sensor corrects the actual sensor, and no big change in the absorbance signal should show.

Figure 4.6 (a) shows the absorbance change of photodiode 1 (PD1) due to the fan turning on and off, without using the reference photodiode 4 (PD4) reading. The absorbance shown is calculated using the following formula:

$$A_1 = -log_{10}(\frac{I_{PD1}}{Constant})$$

And we can see that the fan on and off switch induced absorbance change is about 0.0225, which is comparable to our chemical reaction signal. And if it's not corrected, it will largely effect our sensor readings.

Figure 4.6(b) shows the absorbance of PD1 with the reference PD4 reading taking into account. So this time:

$$A_1 = -log_{10}(\frac{I_{PD1}}{I_{PD4}})$$

And this time, the fan on and off switch induced absorbance change is about 0.0001, which is significantly smaller than our chemical reaction signal, and therefore can be neglected.

By using the reference method, the light source drift, circuit warm up drift and environmental change are corrected. The rejection ratio shown in the example above is 225 times. Such a high reference rejection ratio is very helpful when ppb level detection is desired.

4.2.3 The wired communication interface

As mentioned above, this platform incorporates two kinds of communication interface: a Bluetooth wireless communication and a wired cable communication.

Figure 4.7 shows the connector used in the wired communication between the device and the iPhone. The cable is called male to male 3.5 mm headphone cable, it has two of such connectors on the both ends of the cable, and one goes into the iPhone headphone jack, and one goes into the device female receptor. One connector contains a ground, a left channel, a right channel and a mic.

Figure 4.8 shows the circuit schematic of the data transmission from the device to the iPhone. The mic channel is used here. A general input/output pin of the microcontroller is used to generate the information, it can either output 3 V or 0 V, by altering its output, digital numbers can be represented, the details of this algorithm will be explained later. From the microcontroller pin to the mic of the iPhone, there is a RC filter. This filter is here for two purposes. First it blocks the DC components from the microcontroller. And we do this because the iPhone headphone jack is AC coupled, and for it to recognize that a headphone cable has been plugged in, a capacitor is needed. Second, this RC network lowers the voltage seen by the iPhone. Upon test, we find out that the iPhone mic doesn't take voltage more than 0.3 V, and the output voltage from a microcontroller pin is 3 V, so it has to be lowered by a voltage divider circuit, which is part of this RC network.

Additionally, this RC band pass filter also filters out the high frequency noise. After this RC filter, the iPhone measures the mic voltage, and recover the digital information.

Figure 4.8 shows the data transmission from the device to the iPhone, and figure 4.9(a) shows how the iPhone triggers the device. This control signal goes through the left channel of the cable. The app in the iPhone generates a 20 Hz sinusoid wave, it goes through a diode first, so the negative part of the sinusoid wave is cut. It then goes through non-inverting configured opamp, being amplified to the positive supply voltage of the opamp, which is 3 V, then feed into the general input/output pin of the microcontroller. This transformation is illustrated in figure 4.9(b). When this 20 Hz sinusoid wave goes through the opamp, because of the high amplification factor, the sinusoid wave will become almost like a square wave with its positive value being 3 V, which is the positive supply voltage of the opamp. Using the interrupt capability of the microcontroller port, it can count the numbers of the high-to-low or low-to-high edges of the square wave and when a preset number of interrupts is reached, the data transmission from the device to the iPhone will begin.

Figure 4.10 shows how the zeros and ones are represented using a microcontroller pin. In this algorithm, each bit lasts a fixed duration of t_0, and during this fixed period, the pin will go high (3 V) for a short period of time (t_1) and then go back to low (0 V), it's so called a pulse. The zeros are represented by one pulse and the ones are represented by two pluses. The iPhone then reads the voltage and decides the bit value by it. For the iPhone to decide the starting point of the first bit, a synchronizing signal is sent at the beginning of the data transmission. The synchronizing signal used here is four continuous pulses, the iPhone app will count the number of the pulses, and when it reaches four, the app will know that the data information is coming next and start to receive and decode it.

Figure 4.11 shows the information received by the iPhone app when the synchronizing signal as well as 16 bits are sent. The 16 bits are “010100110110111”, and its decimal value is 10679. The difference between the three results in figure 4.11 is the synchronizing signal length and the bit length. In each graph, the x-axis shows the sample number from the iPhone. The iPhone app samples the mic voltage at 44.1 KHz, so the time length between each sample point is $\frac{1}{44.1\ KHz}$, which is 22.675 μs.

To determine the optimal synchronizing wave length and bit length, different length parameters are tested. In figure 4.11(a), the synchronizing square wave signal period length is 14 iPhone samples, and the bit length is 120 iPhone samples. And in figure 4.11(b), the values are 1.4 iPhone samples and 12 iPhone samples, respectively. Compare these two figures, one can conclude that figure 4.11(a) presents a better result. The reason is that in figure 4.11(a), for each pulse, the reading reaches the maximum, and the four pulses of the synchronizing signal is easily recognized. However, in figure 4.11(b), only two of the four synchronizing pulses can be seen, and the pulses of the bits cannot reach a consistent maximum reading, which makes it difficult to be recognized by the iPhone app.

However, if parameters in figure 4.11(a) are used, each bit last 120 iPhone samples, which is 2721μs, the data transmission rate would be only 46 Bytes/second, and for 1 KB of data, it would take 21.7 seconds to transmit, which seems a little too long. Figure 4.11(c) shows an optimal solution. Its bit length is 49 iPhone samples, which is 1111.075μs and its data transmission rate would be 112 Bytes/second, and now for 1KB of data, it only takes 9 seconds to transmit, which is much more acceptable.

The unit on the y-axis is an arbitrary unit, and the maximum is 2^{31}, which is the maximum that a signed variable in the iPhone app can represent.

4.2.4 The firmware of the microcontroller

There is only one microcontroller on the device circuit, and it is also the most important part of the circuit. The primary tasks for this microcontroller includes controlling the fan, sampling the photodiode voltage, sending the data to the Bluetooth chip, doing real-time calculation of the raw data and communicating with iPhone through a cable. Besides that, it also controls the power of all the major components of the device, they are Bluetooth chip, fan, LED board and all other circuit components such as opamp. All of these are done through the firmware inside the microcontroller. The microcontroller interrupts make the program react to the hardware of the microcontroller. In this program, four different interrupts are used.

The first two interrupts controls the device on and off. Port 1 pin 1 (P1.1) of the microcontroller MSP430F4794 is connected to the middle terminal of a switch, and it's either connected to 3 V or the ground. When this P1.1 is switched from 3 V to ground, the microcontroller detects a high-to-low edge change, and it sets the "DeviceON" flag in the program to be 0, and disables all the voltage regulators except the one for the microcontroller itself, the LCD will display "OFF", and this is a switch off interrupt. When P1.1 is switched from ground to 3 V, the microcontroller sees a low-to-high edge change, and it will set the "DeviceON" flag to be 1, then enable all the voltage regulators, initialize all the preset parameters.

While the device is turned on, a 0.25 second interrupt is enabled. This interrupt is trigged by another small chip called MSP430F2001 from TI, and it sends 0.25 second duration square wave to the main microcontroller, so the interrupt is trigged every 0.25 second. The Sigma-Delta ADC is working at continuous mode, and the result for each photodiode is accumulated. Upon the trigger of the 0.25 second interrupt, ADC stops its conversion, and goes into the interrupt routine. In which, the fan on and off timer is counted, and the photodiode ADC readings are sent to the Bluetooth. Data processing also happen here, the absorbance is calculated and stored in the memory, and the LCD displays the results at the end of each measurement.

While the device is switched off, the data transmission interrupt is enabled. This interrupt is trigged by the 20 Hz square wave sent from the iPhone, and the interrupt routine calculates the individual bit of each integer that is stored in the memory, and sends it to the iPhone as described above.

4.3 Results and discussion

The described colorimetric device is tested with a NO_2 sensor chip. The coated sensing material is o-phenylenediamine (PDA), its reaction with NO_2 is irreversible with a colored phenazine derivative, which allows NO_2 detection and quantification with this device.

The device with the NO_2 sensor is kept within a closed chamber with 4 liter of volume. Then a certain amount of NO_2 gas is injected into the chamber. This NO_2 comes from a standard NO_2 gas cylinder with 40 ppm concentration. The concentration of NO_2 inside the chamber is then calculated based on the dilution rate.

The device is turned on after 2 minutes when the NO_2 is injected. It automatically performs the 2 minutes fan off and 1 minute fan on sampling routine. Figure 4.12(a) shows the absorbance of the sensor for three consecutive tests under three different NO_2 concentrations: 125 ppb, 218 ppb and 343 ppb. Clear absorbance increase is seen during the sampling time. Figure 4.12(b) shows the calibration curve of the device. The sensitivity is 1.296E-4 absorbance change per ppb NO_2. Given the 1E-4 absorbance noise level, the detection limit for NO_2 would be 2.3 ppb.

4.4 Conclusion

A sensor platform that is suitable for colorimetric sensor application is developed. This badge size device is only 120 mm long, 80 mm wide and 8 mm thick. It has a low noise Sigma-Delta ADC for accurate photodiode sampling, with both wireless Bluetooth and wired cable communication interface with Android phone or iPhone. The wired communication interface works with a cable plugged into the iPhone headphone jack, and can synchronize 1 KB of device memory data within 10 seconds. The platform has a battery to support continuous monitoring of at least 10 hours. The sample is drawn through a tiny fan, instead of a sampling pump, which reduces the weight and size the device. The capability of the device is validated using a NO_2 sensor chip, 2.3 ppb detection limit is achieved with the device. This low cost, small size and weight, high performance and battery powered device with both wireless and wired data transmission capability provides a great platform for colorimetric mobile gas sensing.

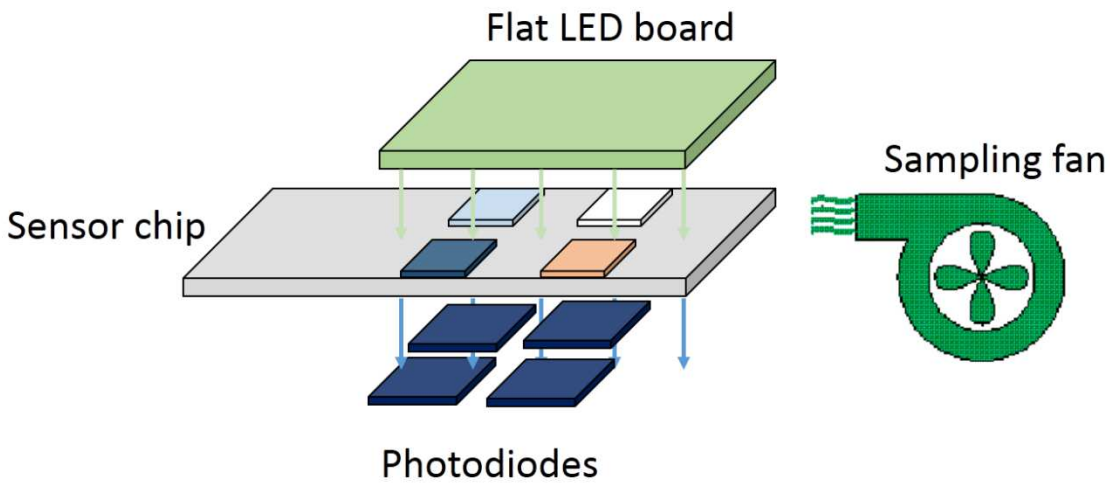

Figure 4-1. The schematic of the colorimetric device.

(a)

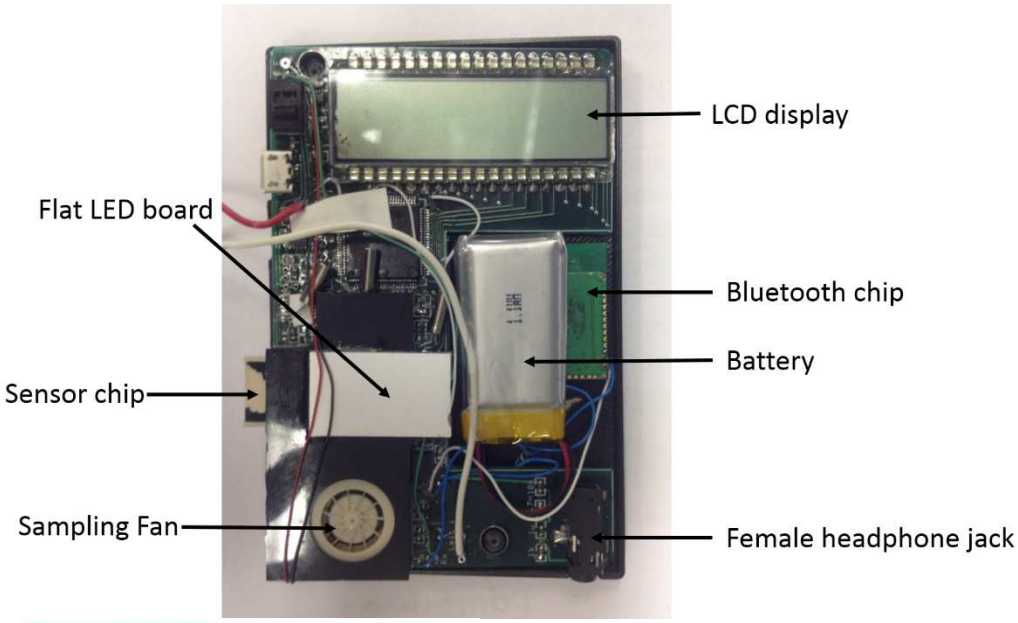

(b)

Figure 4-2. (a) The picture of the device, with marked important components. (b) The picture of the device with the housing.

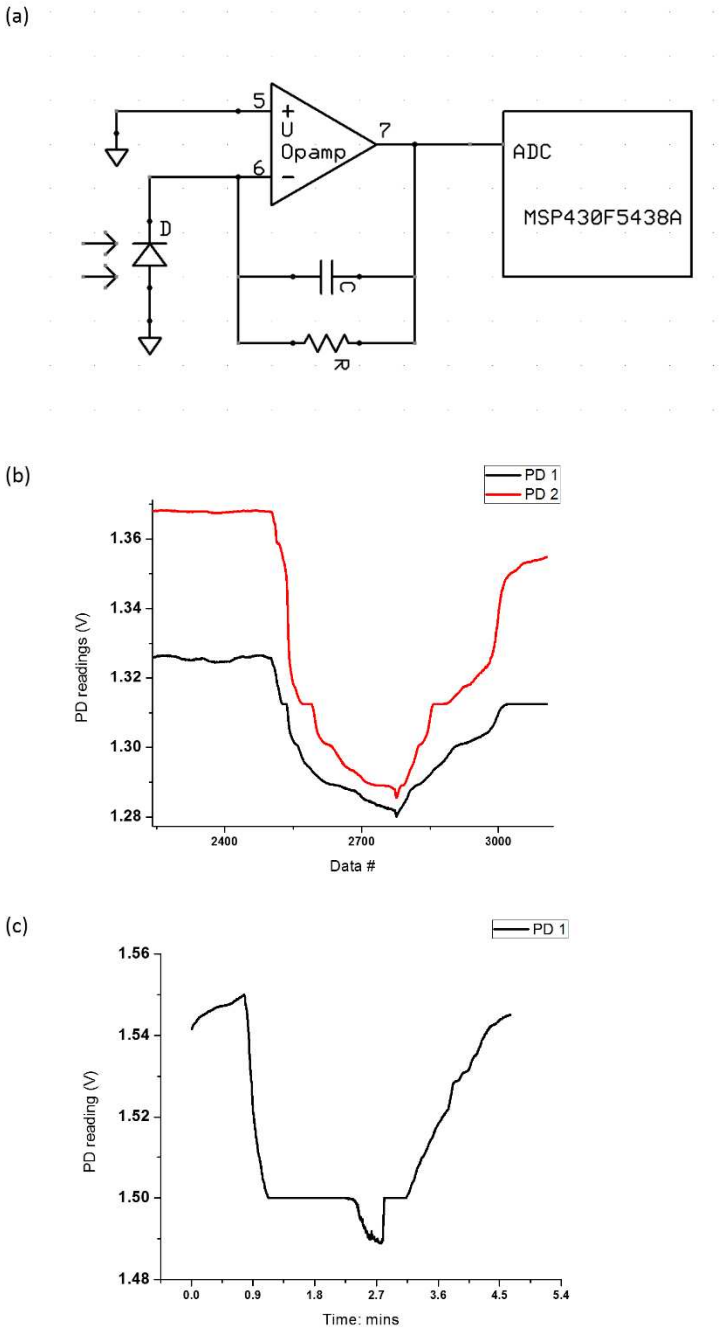

Figure 4-3. (a) The diagram of the photodiode circuit. (b) The repeated value problem of the photodiode reading. (c) The repeated value problem at 1.5 V.

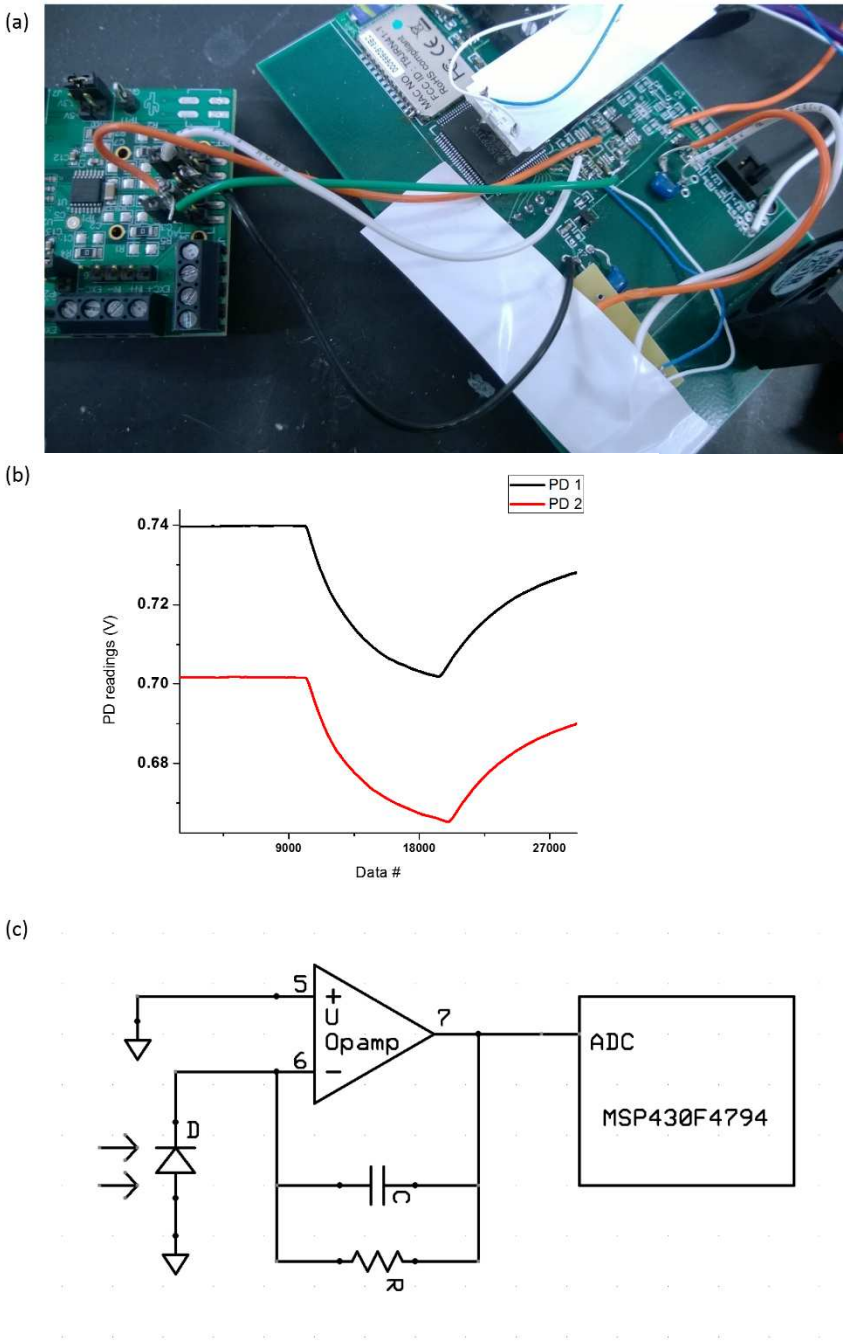

Figure 4-4. (a) Picture of using a Sigma-Delta ADC to measure the photodiode voltage. (b) The results of two photodiodes. (c) The new diagram of the photodiode circuit.

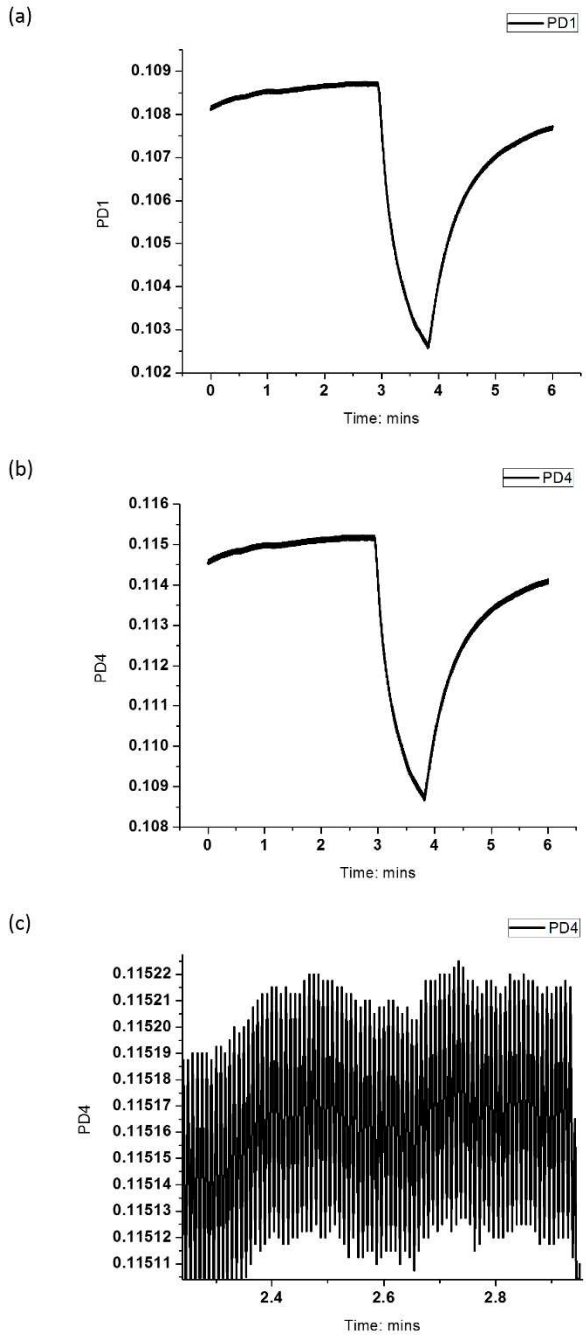

Figure 4-5. (a) The photodiode 1 reading using MSP430F4794 microcontroller with Sigma-Delta ADC. (b) The photodiode 4 reading. (c) The noise level of photodiode 4 reading.

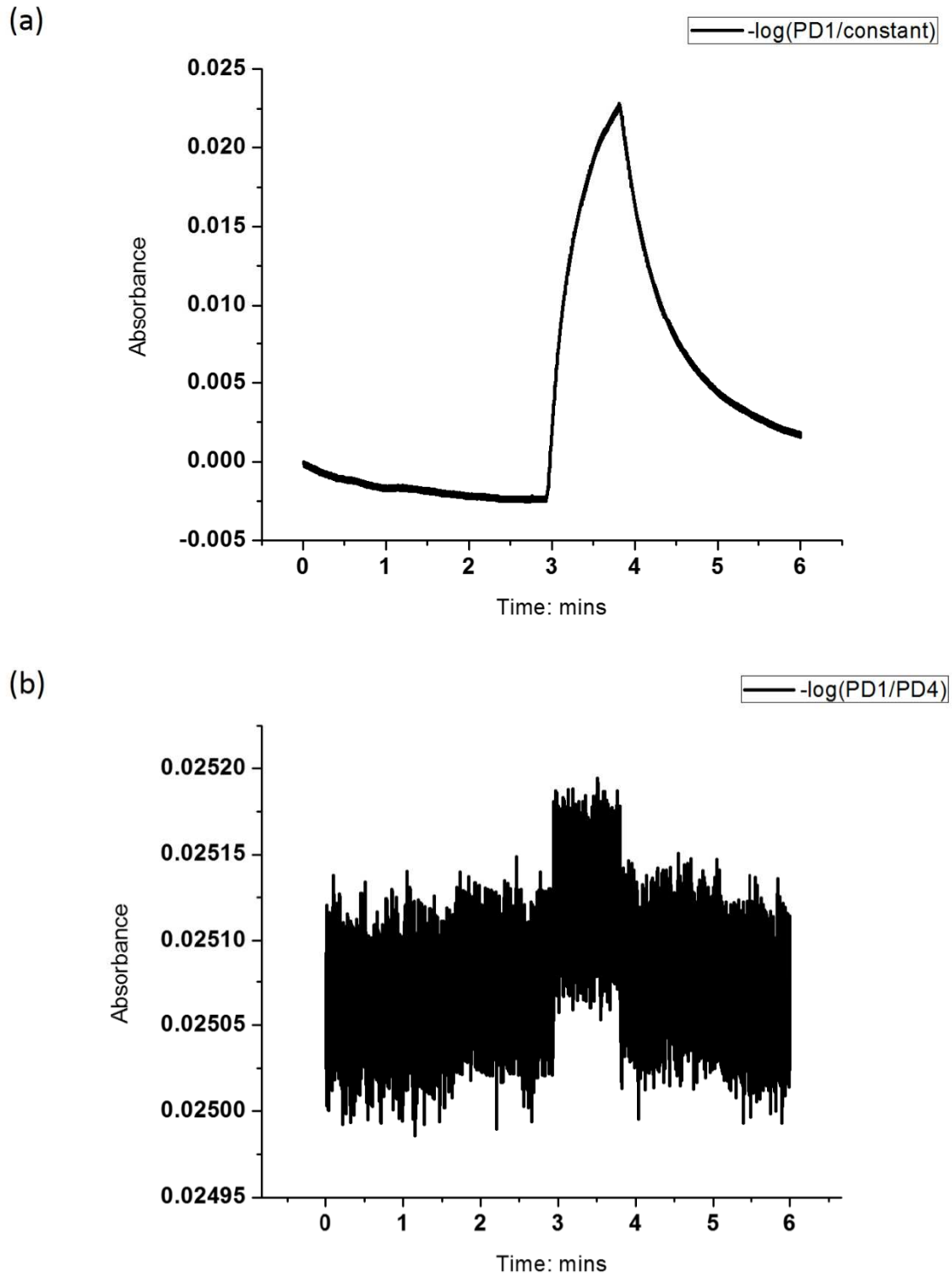

Figure 4-6. (a) Absorbance change without using the reference. (b) Absorbance change with the reference.

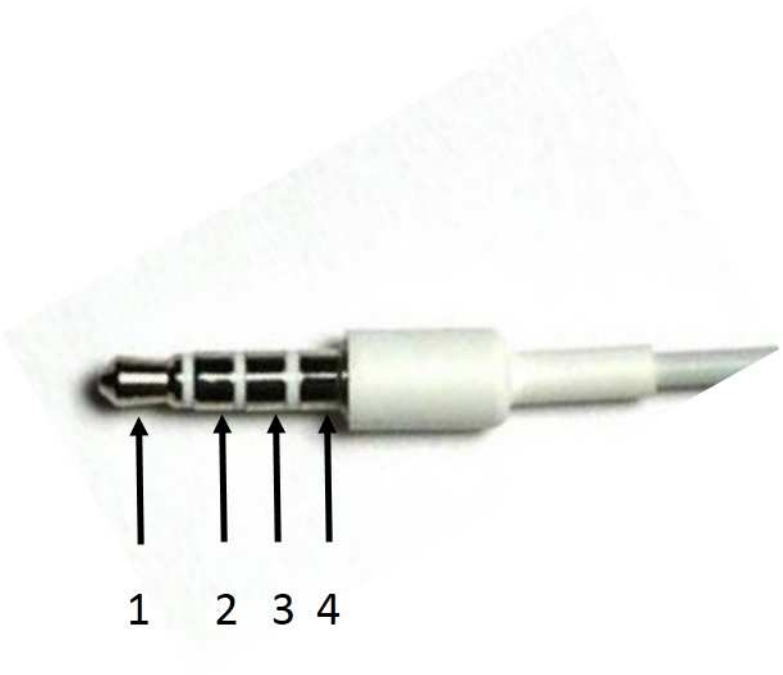

Figure 4-7. The iPhone headphone jack. (1) Left earphone, (2) right earphone, (3) ground, (4) mic.

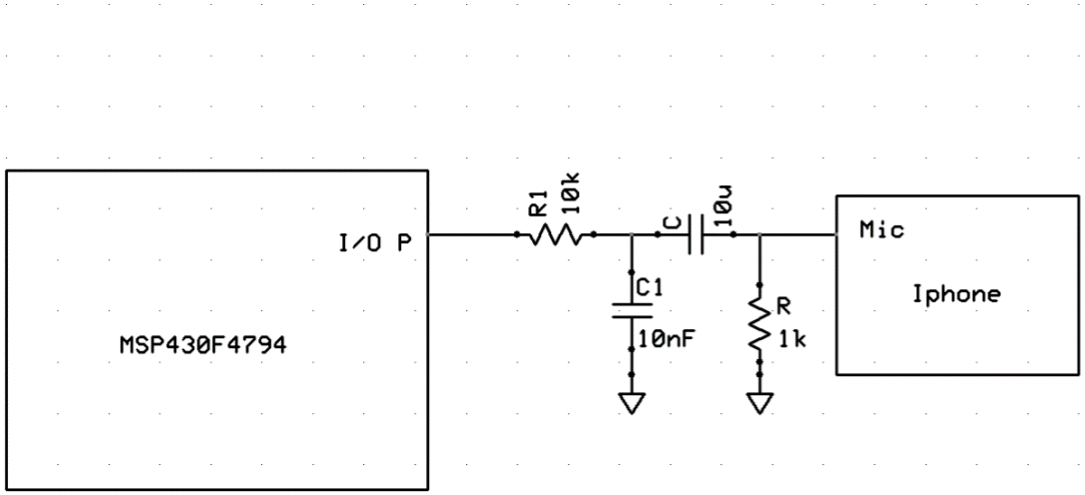

Figure 4-8. The diagram of the data transmission from the device microcontroller to the iPhone.

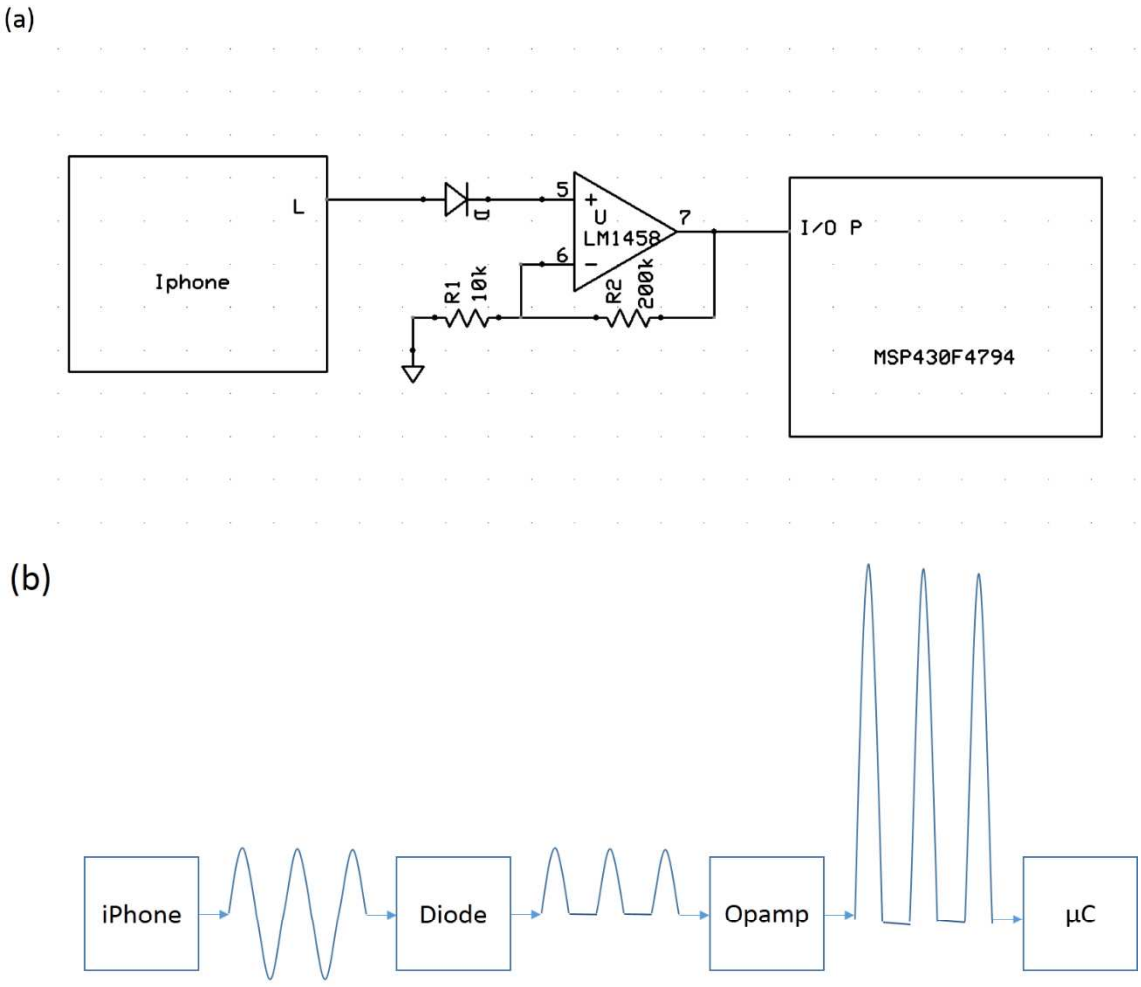

Figure 4-9. (a) The diagram of the control signal from the iPhone to the device microcontroller. (b) Signal transformation diagram.

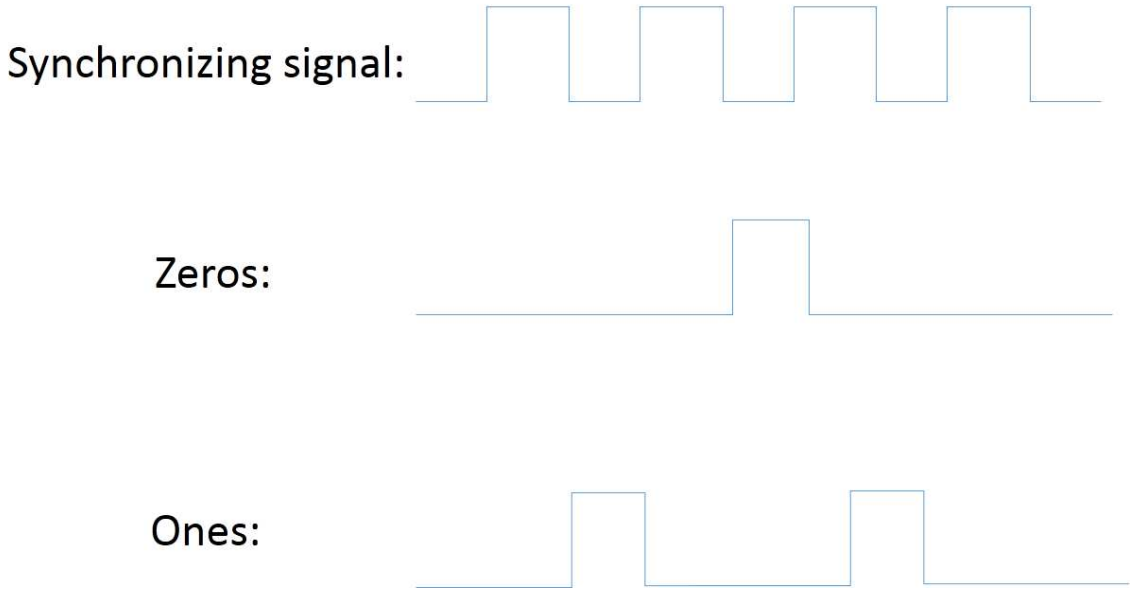

Figure 4-10. The representation of the zeros and ones, as well as the synchronizing signal. The high voltage is 3 V and low voltage is 0 V.

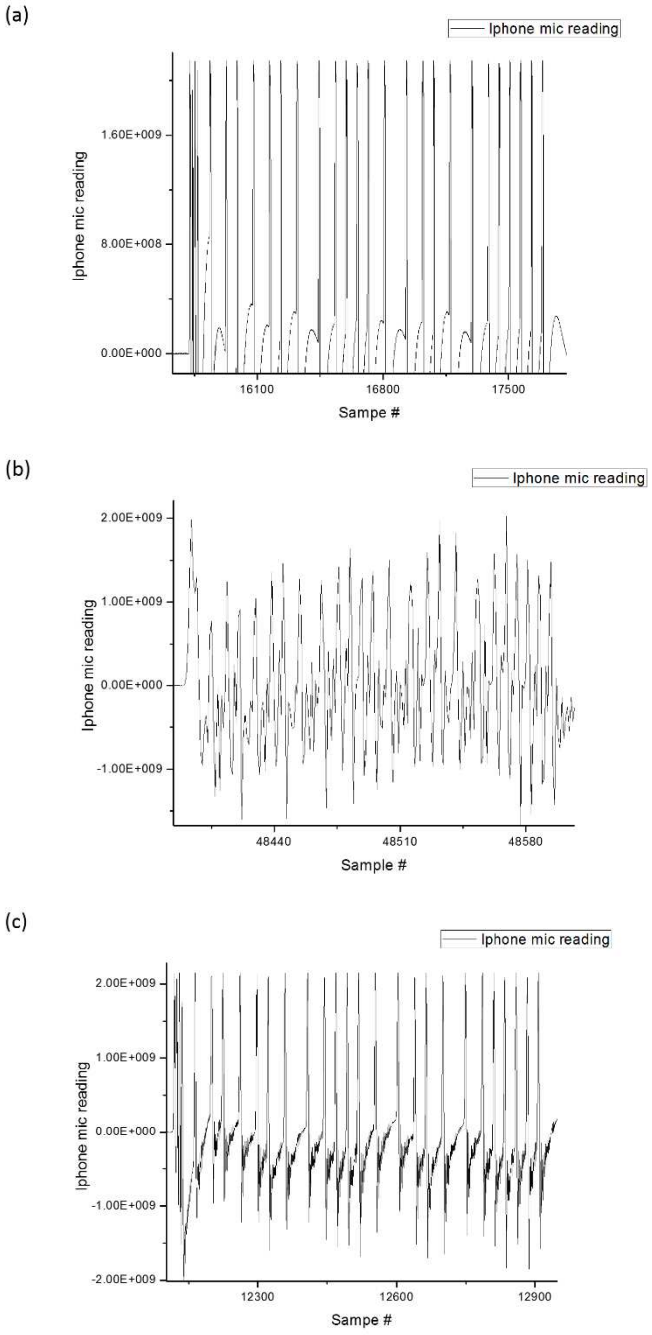

Figure 4-11. Data transmission with different bit length. (a) 2721 μs (b) 272 μs (c) 1111 μs.

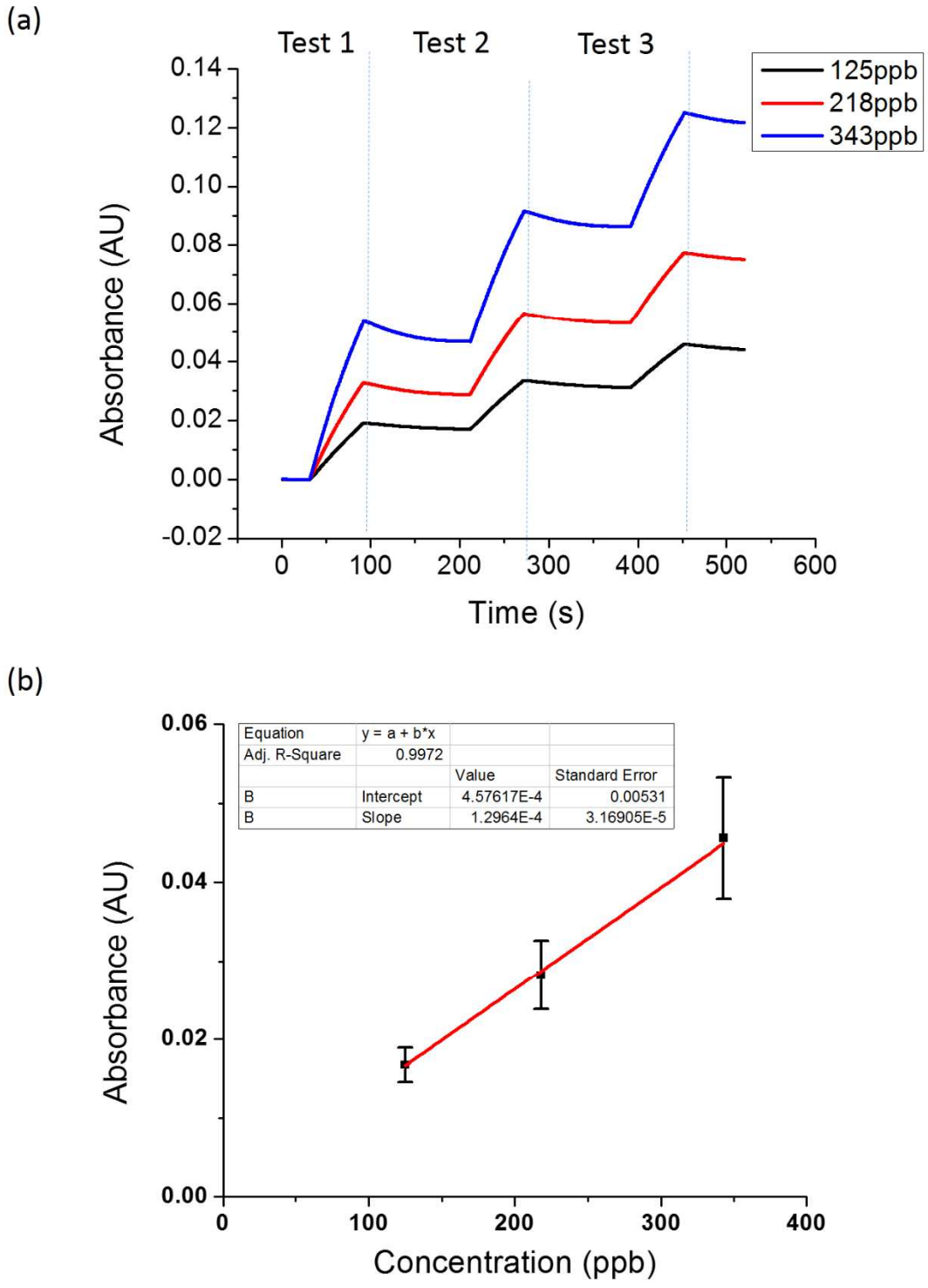

Figure 4-12. (a) Absorbance change of a NO_2 sensor when tested against different NO_2 gas concentrations. (b) The calibration plot.

4.5 Reference

[1] Son, Busoon, et al. "Estimation of occupational and nonoccupational nitrogen dioxide exposure for Korean taxi drivers using a microenvironmental model."*Environmental research* 94.3 (2004): 291-296.

[2] Papke, H., and H. Papen. "Influence of acid rain and liming on fluxes of NO and NO2 from forest soil." *Plant and soil* 199.1 (1998): 131-139.

[3] Yu, Chuck Wah Francis, and Jeong Tai Kim. "Building pathology, investigation of sick buildings—VOC emissions." *Indoor and Built Environment* 19.1 (2010): 30-39.

[4] Suárez, B., et al. "Acute health problems among subjects involved in the cleanup operation following the Prestige oil spill in Asturias and Cantabria (Spain)." *Environmental research* 99.3 (2005): 413-424.

[5] Daisey, Joan M., William J. Angell, and Michael G. Apte. "Indoor air quality, ventilation and health symptoms in schools: an analysis of existing information." *Indoor air* 13.1 (2003): 53-64.

CHAPTER 5

CONCLUSION AND FUTURE WORK

In the previous chapters, three different portable devices have been shown. Two devices are shown for VOCs detection based on a molecularly imprinted polymer coated tuning fork, and one device is shown using the colorimetric detection method. The tuning fork VOC sensor is combined with a gas chromatography column and an adsorbent packed preconcentrator to further increase its sensitivity and selectivity. The integrated device uses four latch valves and one sampling pump, with a Bluetooth enabled circuit, and is capable of detecting ppb level BTEX in real-time. The colorimetric device is only 120 mm long, 80 mm wide and 8 mm thick. It has a low noise Sigma-Delta ADC for accurate photodiode sampling, with both wireless Bluetooth and wired cable communication interface with Android phone or iPhone. It provides a great platform for colorimetric sensor applications.

However, further reduction on the size and cost of the devices are needed for it to be convenient for everyday use. With that, it is even possible to integrate one chemical sensor into a popular smartphone, such as an iPhone, and it could open of a lot of possibilities, such as mobile air quality sensor network.

CHAPTER 6

REFERENCES

Chapter 1

[22] Amorim, Leiliane CA, Joana P. Carneiro, and Zenilda L. Cardeal. "An optimized method for determination of benzene in exhaled air by gas chromatography–mass spectrometry using solid phase microextraction as a sampling technique." *Journal of Chromatography B* 865.1 (2008): 141-146.

[23] Sexton, Ken, et al. "Children's exposure to volatile organic compounds as determined by longitudinal measurements in blood." *Environmental health perspectives* 113.3 (2005): 342.

[24] Han, Xianglu, and Luke P. Naeher. "A review of traffic-related air pollution exposure assessment studies in the developing world." *Environment international* 32.1 (2006): 106-120.

[25] Buczynska, Anna Jolanta, et al. "Atmospheric BTEX-concentrations in an area with intensive street traffic." *Atmospheric Environment* 43.2 (2009): 311-318.

[26] Ablat, Hayrensa, et al. "Nafion film/K+-exchanged glass optical waveguide sensor for BTX detection." *Analytical chemistry* 80.20 (2008): 7678-7683.

[27] De Medeiros, A. P., et al. "Traffic-related air pollution and perinatal mortality: a case-control study." *Environ Health Perspect* 117.1 (2009): 127-132.

[28] Fondelli, M. Cristina, et al. "Benzene exposure in a sample of population residing in a district of Florence, Italy." *Science of the total environment* 392.1 (2008): 41-49.

[29] Harrison, Roy M., et al. "Analysis of incidence of childhood cancer in the West Midlands of the United Kingdom in relation to proximity to main roads and petrol stations." *Occupational and Environmental Medicine* 56.11 (1999): 774-780.

[30] Raaschou‐Nielsen, Ole, and Peggy Reynolds. "Air pollution and childhood cancer: a review of the epidemiological literature." *International journal of cancer*118.12 (2006): 2920-2929.

[31] Tsai, S., H. Weng, and C. Yang. "Association of Childhood Leukemia with Residential Exposure to Petrochemical Air Pollution in Taiwan." *Epidemiology*19.6 (2008): S292.

[32] Weng, Hsu-Huei, et al. "Childhood leukemia and traffic air pollution in Taiwan: petrol station density as an indicator." *Journal of Toxicology and Environmental Health, Part A* 72.2 (2008): 83-87.

[33] Whitworth, Kristina W., Elaine Symanski, and Ann L. Coker. "Childhood lymphohematopoietic cancer incidence and hazardous air pollutants in southeast Texas, 1995–2004." (2008).

[34] Infante-Rivard, Claire. "Chemical risk factors and childhood leukaemia: a review of recent studies†." *Radiation protection dosimetry* 132.2 (2008): 220-227.

[35] http://www.raesystems.

[36] www.draeger.com

[37] www.agilent.com/chem/microgc.

[38] www.hnu.com.

[39] www.photovac.com.

[40] http://microsensorsystems.com.

[41] http://www.estcal.com.

[42] Lu, Chia-Jung, et al. "First-generation hybrid MEMS gas chromatograph." *Lab on a Chip* 5.10 (2005): 1123-1131.

Chapter 2

[30] de Medeiros, A. P. P.; Gouveia, N.; Machado, R. P. P.; de Souza, M. R.; Alencar, G. P.; Novaes, H. M. D.; de Almeida, M. F., Traffic-Related Air Pollution and Perinatal Mortality: A Case Control Study. Environmental Health Perspectives 2009, 117, (1), 127-132.

[31] Fondelli, M. C.; Bauazzano, P.; Grechi, D.; Gorini, G.; Miligi, L.; Marchese, G.; Cenni, I.; Scala, D.; Chellini, E.; Costantini, A. S., Benzene exposure in a

sample of population residing in a district of Florence, Italy. Science Of The Total Environment 2008, 392, (1), 41-49.

[32] Han, X. L.; Naeher, L. P., A review of traffic-related air pollution exposure assessment studies in the developing world. Environment International 2006, 32, (1), 106-120.

[33] Harrison, R. M.; Leung, P. L.; Somervaille, L.; Smith, R.; Gilman, E., Analysis of incidence of childhood cancer in the West Midlands of the United Kingdom in relation to proximity to main roads and petrol stations. Occupational And Environmental Medicine 1999, 56, (11), 774-780.

[34] Raaschou-Nielsen, O.; Reynolds, P., Air pollution and childhood cancer: A review of the epidemiological literature. International Journal Of Cancer 2006, 118, (12), 2920-2929.

[35] Tsai, S.; Weng, H.; Yang, C., Association of Childhood Leukemia with Residential Exposure to Petrochemical Air Pollution in Taiwan. Epidemiology 2008, 19, (6), S292-S292.

[36] Weng, H. H.; Tsai, S. S.; Chiu, H. F.; Wu, T. N.; Yang, C. Y., Childhood Leukemia and Traffic Air Pollution in Taiwan: Petrol Station Density as an Indicator. Journal Of Toxicology And Environmental Health-Part A-Current Issues 2009, 72, (2), 83-87.

[37] Whitworth, K. W.; Symanski, E.; Coker, A. L., Childhood Lymphohematopoietic Cancer Incidence and Hazardous Air Pollutants in Southeast Texas, 1995-2004. Environmental Health Perspectives 2008, 116, (11), 1576-1580.

[38] Infante-Rivard, C., Chemical risk factors and childhood leukaemia: a review of recent studies dagger. Radiation Protection Dosimetry 2008, 132, (2), 220-227.

[39] Buczynska, A. J.; Krata, A.; Stranger, M.; Godoi, A. F. L.; Kontozova-Deutsch, V.; Bencs, L.; Naveau, I.; Roekens, E.; Van Grieken, R., Atmospheric BTEX-concentrations in an area with intensive street traffic. Atmospheric Environment 2009, 43, (2), 311-318.

[40] Ablat, H.; Yimit, A.; Mahmut, M.; Itoh, K., Nafion film/K+-exchanged glass optical waveguide sensor for BTX detection. Analytical Chemistry 2008, 80, (20), 7678-7683.

[41] www.defiant-tech.com

[42] www.slsmt.com

[43] www.c2v.nl

[44] www.hnu.com

[45] www.photovac.com

[46] Chia-Jung, L.; Steinecker, W. H.; Tian, W. C.; Oborny, M. C.; Nichols, J. M.; Agah, M.; Potkay, J. A.; Chan, H. K. L.; Driscoll, J.; Sacks, R. D.; Wise, K. D.; Pangad, S. W.; Zellers, E. T. Lab Chip 2005, 5, 1123–1131.

[47] Zhong, Q.; Steinecker, W. H.; Zellers, E. T. Analyst 2009, 134, 283.

[48] Zampolli, S.; Elmi, I.; Sturmann, J.; Nicoletti, S.; Dori, L.; Cardinali, C. Sens. Actuators, B: Chem. 2005, 105, 400–406.

[49] Zampolli, S.; Elmi, I.; Mancarella, F.; Betti, P.; Dalcanale, E.; Cardinali, . C.; Severi, M. Sens. Actuators, B 2009, 141, 322.

[50] Iglesias, R.; Tsow, F.; Wang, R.; Forzani, E.S.; Tao, N.J.; Anal. Chem. 2009, 81(21)8930-8935.

[51] Ren, M. H.; Forzani, E. S.; Tao, N. J. Anal. Chem. 2005, 77, 2700–2707.

[52] Tsow, F.; Forzani, E. S.; Tao, N. J. Anal. Chem. 2008, 80, 606–611.

[53] Tsow, F.; Tao, N. Appl. Phys. Lett. 2007, 90, 174102.

[54] Ren, M. H.; Tsow, T.; Forzani, E. S.; Tao, N. J. Abstr. Pap. Am. Chem. Soc. 2005, 229, 396-ANYL.

[55] Negi, I.; Tsow, F.; Tanwar, K.; Zhang, L.; Iglesias RA.; Chen, C.; Rai, A.; Forzani, ES.; Tao, N.; "Novel monitor paradigm for real-time exposure assessment", Journal of Exposure Science and Environmental Epidemiology, jes.2010.35.

[56] Solomon, G.; Janssen, S.; JAMA, 2010, Vol 304, No. 10, 1118-1119.

[57] Ellman, M.; Navarr O, K.; Solomon, G.; Environ. Sci. Technol. 2010, 44, 8365–8366.

[58] Sacks, R.; Klemp, M.; Akard, M. Field Anal. Chem. Technol. 1996, 1, 97–102.

Chapter 3

[31] Amorim, Leiliane CA, Joana P. Carneiro, and Zenilda L. Cardeal. "An optimized method for determination of benzene in exhaled air by gas chromatography–mass spectrometry using solid phase microextraction as a sampling technique." *Journal of Chromatography B* 865.1 (2008): 141-146.

[32] Sexton, Ken, et al. "Children's exposure to volatile organic compounds as determined by longitudinal measurements in blood." *Environmental health perspectives* 113.3 (2005): 342.

[33] Han, Xianglu, and Luke P. Naeher. "A review of traffic-related air pollution exposure assessment studies in the developing world." *Environment international* 32.1 (2006): 106-120.

[34] Buczynska, Anna Jolanta, et al. "Atmospheric BTEX-concentrations in an area with intensive street traffic." *Atmospheric Environment* 43.2 (2009): 311-318.

[35] Ablat, Hayrensa, et al. "Nafion film/K+-exchanged glass optical waveguide sensor for BTX detection." *Analytical chemistry* 80.20 (2008): 7678-7683.

[36] De Medeiros, A. P., et al. "Traffic-related air pollution and perinatal mortality: a case-control study." *Environ Health Perspect* 117.1 (2009): 127-132.

[37] Fondelli, M. Cristina, et al. "Benzene exposure in a sample of population residing in a district of Florence, Italy." *Science of the total environment* 392.1 (2008): 41-49.

[38] Harrison, Roy M., et al. "Analysis of incidence of childhood cancer in the West Midlands of the United Kingdom in relation to proximity to main roads and petrol stations." *Occupational and Environmental Medicine* 56.11 (1999): 774-780.

[39] Raaschou‐Nielsen, Ole, and Peggy Reynolds. "Air pollution and childhood cancer: a review of the epidemiological literature." *International journal of cancer*118.12 (2006): 2920-2929.

[40] Tsai, S., H. Weng, and C. Yang. "Association of Childhood Leukemia with Residential Exposure to Petrochemical Air Pollution in Taiwan." *Epidemiology*19.6 (2008): S292.

[41] Weng, Hsu-Huei, et al. "Childhood leukemia and traffic air pollution in Taiwan: petrol station density as an indicator." *Journal of Toxicology and Environmental Health, Part A* 72.2 (2008): 83-87.

[42] Whitworth, Kristina W., Elaine Symanski, and Ann L. Coker. "Childhood lymphohematopoietic cancer incidence and hazardous air pollutants in southeast Texas, 1995–2004." (2008).

[43] Infante-Rivard, Claire. "Chemical risk factors and childhood leukaemia: a review of recent studies†." *Radiation protection dosimetry* 132.2 (2008): 220-227.

[44] http://www.raesystems.

[45] www.draeger.com

[46] www.agilent.com/chem/microgc.

[47] www.hnu.com.

[48] www.photovac.com.

[49] http://microsensorsystems.com.

[50] http://www.estcal.com.

[51] Lu, Chia-Jung, et al. "First-generation hybrid MEMS gas chromatograph." *Lab on a Chip* 5.10 (2005): 1123-1131.

[52] Tsow, Francis, et al. "A wearable and wireless sensor system for real-time monitoring of toxic environmental volatile organic compounds." *Sensors Journal, IEEE* 9.12 (2009): 1734-1740.

[53] Iglesias, Rodrigo A., et al. "Hybrid separation and detection device for analysis of benzene, toluene, ethylbenzene, and xylenes in complex samples."*Analytical chemistry* 81.21 (2009): 8930-8935.

[54] Chen, Cheng, et al. "A wireless hybrid chemical sensor for detection of environmental volatile organic compounds." (2011): 1-1.

[55] Chen, Cheng, et al. "A new sensor for the assessment of personal exposure to volatile organic compounds." *Atmospheric environment* 54 (2012): 679-687.

[56] Negi, Indira, et al. "Novel monitor paradigm for real-time exposure assessment."*Journal of Exposure Science and Environmental Epidemiology* 21.4 (2011): 419-426.

[57] Lane, Nicholas D., et al. "BeWell: A smartphone application to monitor, model and promote wellbeing." *5th International ICST Conference on Pervasive Computing Technologies for Healthcare*. 2011.

[58] Kirwan, Morwenna, et al. "Using smartphone technology to monitor physical activity in the 10,000 Steps Program: a matched case–control trial." *Journal of medical Internet research* 14.2 (2012).

[59] Lam, Stephen Chiu Kwok, et al. "A smartphone-centric platform for personal health monitoring using wireless wearable biosensors." *Information, Communications and Signal Processing, 2009. ICICS 2009. 7th International Conference on*. IEEE, 2009.

[60] http://www.sigmaaldrich.com/catalog/product/supelco/10436?lang=en&region=US.

Chapter 4

[6] Son, Busoon, et al. "Estimation of occupational and nonoccupational nitrogen dioxide exposure for Korean taxi drivers using a microenvironmental model."*Environmental research* 94.3 (2004): 291-296.

[7] Papke, H., and H. Papen. "Influence of acid rain and liming on fluxes of NO and NO2 from forest soil." *Plant and soil* 199.1 (1998): 131-139.

[8] Yu, Chuck Wah Francis, and Jeong Tai Kim. "Building pathology, investigation of sick buildings—VOC emissions." *Indoor and Built Environment* 19.1 (2010): 30-39.

[9] Suárez, B., et al. "Acute health problems among subjects involved in the cleanup operation following the Prestige oil spill in Asturias and Cantabria (Spain)." *Environmental research* 99.3 (2005): 413-424.

[10] Daisey, Joan M., William J. Angell, and Michael G. Apte. "Indoor air quality, ventilation and health symptoms in schools: an analysis of existing information." *Indoor air* 13.1 (2003): 53-64.

[11] Summit, Earth. "Health and environment in sustainable development." (1997).